TÉCNICO LISBOA

Thermal Model Development of Modular Data Centers for Calibration and Multi-Objective Optimization

Sören Friedrichs

Thesis to obtain the Master of Science Degree in

Energy Engineering and Management

Supervisors: Prof. Carlos Augusto Santos Silva
Eng. Henrique Ramalho Monteiro Latourrette Pombeiro

Examination Committee

Chairperson: Prof. Edgar Caetano Fernandes
Supervisor: Prof. Carlos Augusto Santos Silva
Member of the Committee: Drª. Diana Pereira Neves

November 2017

Acknowledgements

This thesis represents the completion of my studies at IST. Hereinafter I would like to thank the persons that supported me in this work and during my university career.

Special gratitude to Henrique Pombeiro and Professor Carlos Silva for their continuous support, precious input and helpful guidance.

Moreover, thanks to Ricardo Gomes for assisting me in issues with EnergyPlus.

I would also like to thank the expert in building optimization and developer of the tool jEPlus, Dr. Yi Zhang, who gave me some helpful advices and free simulation time for JESS.

Thank you, Catarina, for teaming up and positive vibes.

Finally, I would like to thank my family and friends, which gave me the opportunity to study and which were always supporting me in my decisions.

Abstract

The use of containerized Modular Data Centers (MDCs) is an ongoing emerging trend within the industry and is gradually increasing, due to growing demand for cloud services. Consequently, the energy impact of these system is increasing significantly. Compared to traditional data centers, modular data centers are standardized, rapidly fabricated and quickly deployed. The purpose of modular data centers is to store and process data for telecommunications, Internet providers or IT companies.

The aim of this thesis is to improve energy performance of four remote MCDs distributed across Portugal. As data center equipment generally generates enormous amounts of heat, HVAC systems are permanently required to cool down the data center space. This study develops and calibrates thermal models for the data center facilities based on real time temperature and energy consumption measurements in the software EnergyPlus. Two locations were successfully validated for time periods of three weeks with only minor discrepancies between measured and simulated values.

Based on these calibrated solutions, two multi-objective optimization models were created with the software jEPlus. The models merge six individual optimization solutions, such as free-cooling or shading devices. The purpose is to determine the best combinations of solutions that minimize investment costs and energy costs. Results for solutions with highest investment costs show significant energy cost savings and energy consumption reductions (15.2% and 13.3%) for both models in a tri-rate time energy tariff compared to the calibrated cases (simple tariff). However, solutions with low investment costs can still substantially reduce energy consumption and costs.

Keywords

Modular data center, building energy simulation, building calibration, multi-objective optimization

Resumo

O uso de data centers contentorizadas modulares é uma tendência emergente dentro da industria e está a aumentar gradualmente, devido à crescente procura de serviços em cloud. Consequentemente, o impacto energético destes sistemas está a aumentar significativamente. Em comparação com data centers tradicionais, os data centers modulares são padronizados, rapidamente fabricados e implantados. O propósito dos data centers modulares é armazenar e processar dados para telecomunicações, fornecedores de internet e empresas de IT.

O objetivo desta tese é melhorar o desempenho energético de quatro data centers modulares remotos distribuídos em Portugal. Como o equipamento presente no data center geralmente gera grandes quantidades de calor, os sistemas HVAC são necessários para arrefecer permanentemente o seu espaço interior. Este estudo desenvolve e calibra modelos térmicos para as instalações do data center com base em medidas de temperatura e consumo de energia em tempo real usando o software EnergyPlus. Dois locais foram validados com sucesso para períodos de três semanas com apenas pequenas discrepâncias entre valores medidos e simulados.

Com base nessas soluções calibradas, dois modelos de otimização multi-objetivo foram criados com o software jEPlus. Os modelos combinam seis soluções individuais de otimização, como free-cooling ou de sombreamento. O objetivo é determinar as melhores combinações de soluções que minimizam custos de investimento e de energia. Os resultados para soluções com os maiores custos de investimento mostram poupanças significativa de custos de energia e reduções de consumo de energia (15.2% e 13.3%) para ambos os modelos com uma tarifa tripla de energia em comparação com os casos calibrados (tarifa simples). No entanto, soluções com baixos custos de investimento podem ainda reduzir substancialmente o consumo de energia e os custos.

Palavras-chave:
data centers modulares, simulação de energia em edificios, building calibration, otimização multi-objetivo

Table of Contents

List of Acronyms

ACH	= Air Changes per Hour
CRAC	= Computer Room Air Conditioner
CV(RMSE)	= Coefficient of Variance of Root Mean Square Error
DCIE	= Data Center Infrastructure Efficiency
DX	= Direct Expansion
EA	= Evolutionary Algorithms
HVAC	= Heating Ventilation and Air Conditioning
ICT	= Information and Communication Technology
JESS	= jEPlus Simulation Server
MDC	= Modular Data Center
MOO	= Multi-Objective Optimization
NMBE	= Normalized Mean Bias Error
PTAC	= Packaged Terminal Air Conditioner
PUE	= Power Usage Effectiveness
TMY	= Typical Meteorological Year
UPS	= Uninterruptable Power Supply

List of Figures

List of Tables

1 Introduction

1.1 Motivation

The development of society is creating an increasingly intensive usage of Internet, social media and cloud-based computing. The current social habits generate massive amount of information, such as videos, audios, emails, status updates, news or tweets. This big data needs to be stored and processed continuously in facilities named data centers.

Facilities for Information and Communications Technology (ICT) consume significant amounts of electricity, representing around 1.5% to 2% of the world's consumed energy in 2014 with a growth rate of about 12% per year [1], [2]. Data centers can consume 100-200 times more electricity as normal office spaces and must run nonstop 8760 hours per year. One significant part of the utilized electricity is released as heat in the processing units that needs to be removed by air-conditioning systems to keep the data processing units cool at any point of time. This represents also a large part of the total facility's energy consumption. Data centers are thus becoming rapid growing consumers of energy and are in the focus for energy-efficient design measures [3].

Global electricity demand from data centers is expected to be two to three times higher in the year 2020 compared to the year 2007. Recent scenarios anticipate that worldwide data center energy consumption will reach 507.9 TWh by the year 2020 [2] considering an average data center efficiency. Implementing efficient technologies may decrease this number by 12.4% and could counteract the increasing demand for cloud-based connectivity.

A more recent evolution on the data center construction market is a type called Modular Data Centers (MDCs). These containerized modules are especially meaningful for remote or temporary installations. In 2012, this type of build represented less than 5% of the total market, but it has been projected to increase rapidly for the next several years.

Under the Energy Efficient Directive, all EU countries are required to use energy more efficiently at all stages of the energy chain, from production to final consumption. Heating and cooling in buildings and industry accounts for half of the EU's energy consumption. Moreover, 82% of heating and cooling is still generated from fossil fuels, while only 18% is generated from renewable energy [4]. To achieve the EU's climate and energy goals, in particular increasing energy efficiency by 27%, the heating and cooling sector must severely reduce its energy consumption and clean energy needs to become the primary source. These goals also concern the ICT infrastructure sector.

1.2 Research Problem and Objective

The research problem of this thesis is to improve energy efficiency of different operating remote Modular Data Centers (MDCs), due to their significant energy consumption caused by high and steady cooling needs. In this thesis, energy consumption in the MDCs refer to electricity consumption. Typically, those MDCs are containers equipped with Information and Communication Technology (ICT) equipment such as servers or other communication systems where part of the power capacity is transformed into heat. This heat needs to be removed by HVAC systems to ensure a controlled atmosphere (temperature, humidity and dust). In this case study, these facilities are used for telecommunication purposes and are distributed throughout four locations in Portugal. The objective of this work is to create and validate a thermal simulation model of the MDCs only based on real time measurements in a first step. Information about ICT equipment and air conditioning settings are not available. This reconciliation of model outputs with measured data is known as calibration. A calibrated model allows the forecast and estimation of cooling needs depending on climatic conditions. Consequently, in a next step the performance of a calibrated thermal model may be improved by employing appropriate solutions embedded in a multi-objective optimization (MOO) problem.

1.3 Structure and Approach

This study is organized in six chapters. The approach of the thesis is shown in Figure 1-1.

Figure 1-1: Approach of the thesis

In the first chapter the motivation and the subsequent research problem and goal of this thesis are introduced.

The second chapter briefly characterizes the functions and technical development of modular data centers. Moreover, it explains applied cooling techniques, actual intelligent energy management solutions and the appropriate room climate for data centers. In addition, the theoretical fundamentals of heat transfer for the simulation models are given.

The third chapter describes the whole thermal simulation *model development.* As a preparation for the model development, measurement, weather data and additional facility *data is processed* before.

The forth chapter introduces the *calibration of the models*. The calibration method is split in a manual and an automated calibration. Additionally, a sensitivity analysis of the calibration is performed.

In the fifth chapter a *model optimization* is presented. Initially, individual solutions to increase the energy performance are explored. Then, multi-objective optimization models are created, to *evaluate* the best combinations of solutions.

In the sixth chapter, the main outcomes of this thesis are presented, showing the quality and vulnerabilities of the simulation models. Finally, an outlook on possible adjustments and prospective tasks is given.

2 Fundamentals of Modular Data Centers

This chapter introduces the fundamentals of modular data centers considering market evolution, recent technical developments and cooling methods. Current solutions for intelligent energy management for data centers are also presented, as well as the theoretical basis for the heat transfer inside and outside of the data center containers is described.

2.1 Modular Data Center

Modular Data Centers (MCDs) emerged in 2007 [5] and are now offered by many manufacturers. They are used in a big scale for cloud computing in companies like Microsoft [6] or Google [7] and for small installations throughout the industry. Various hardware suppliers started to build their own container versions, such as Huawei [8], HPE [9] or Dell [10], [11]. According to [2], containerized data centers are undergoing an increasing demand on the market. Since 2014 the market is increasing significantly with a proposed growth of more than 20% until 2020. The trend from 2010 to 2020 is printed in Figure 2-1.

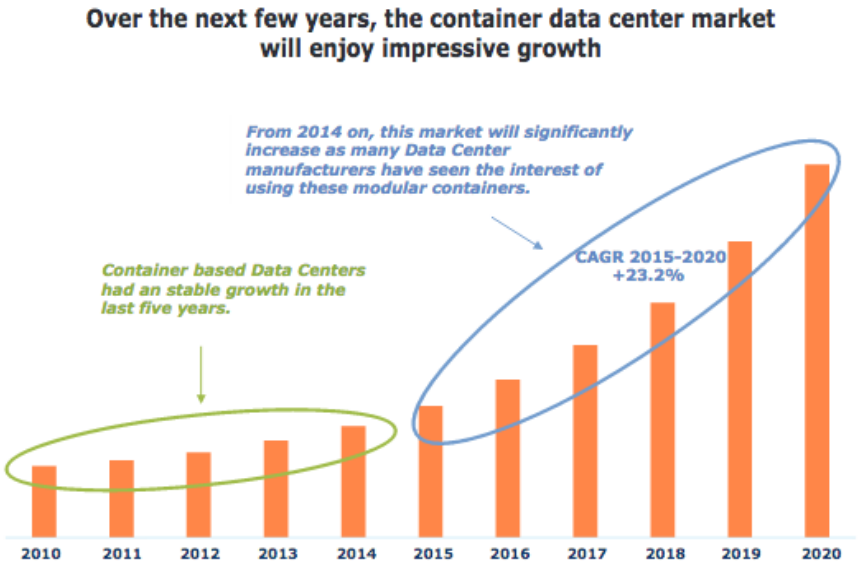

Figure 2-1: Data center market evolution 2010 to 2020 [2]

The purpose of modular data centers is the data storage and processing for telecommunications, Internet provider or IT companies. They are equipped with servers, network equipment, energy and temperature monitoring systems as well as UPS (Uninterruptible Power Supply), backup power and eventually a fire protection system. The UPS ensures that the supply remains constant. It compensates for voltage and frequency fluctuations and thereby effectively protects sensitive computer electronic components and systems.

Often standard shipping containers with ISO standards are used as the enclosure for those data center units. Standard sizes for these containers are: 20 ft. (6058 x 2438 x 2591 mm) or 40 ft. (12192 x 2438 x 2591 mm). Usually there are cutouts in the envelope for doors or other mountings that hang off the side or are placed on top. Their advantages are a rapid fabrication; a robust envelope, lower construction costs, an easy transport and a quick deployment that saves time and costs compared to regular brick and mortar data centers [12], [13]. The modules can be shipped and assembled anywhere to fulfill the customer's needs. Another benefit can be the efficiency, if they are properly sized regarding cooling equipment and utilization rates. Whenever there is a need, additional units can be incorporated into a given data center structure to increase overall capacity.

In this thesis only "all-in-one" data centers are analyzed. As the name already explains, all components (Power, Cooling and IT) are set up in a single structure, thus the power capacity is typically less than 150 kW [14]. The average power density in high-density data centers is 1.5 kW/m^2 [15]. Modular data centers are especially meaningful for the usage in regions where grid connected brick and mortar data centers cannot be built or for scaling up the capacity of existing data center infrastructure. As a result of their good mobility, containerized data centers have to deal with a wide range of climates, thus the cooling systems are dimensioned to handle different conditions. Most MCDs are placed outdoors, thus they are designed to match local requirements for extreme temperatures or snow loads. Insulation should prevent solar gains in a sunny environment, but more important insulation is needed in winter. It is critical to start IT Servers below 10°C. Once they run, their waste heat prevents a cold environment [16]. Typically, their energy needs for cooling tend to be around 20% to 50%, which require check and control to limit their energy consumption. Accompanied by the goal of energy reduction is the focus of the industry to minimize the negative environmental impact of data centers.

2.2 Space Climate in Data Centers

The American Society of Heating, Refrigerating, and Air-conditioning Engineers (ASHRAE) publishes guidelines for temperature and humidity operating ranges of IT equipment in data centers [17]. Figure 2-2 gives an insight of the different operating classes. The recommended operating envelope is the same for all classes while the allowable envelope is changing within the classes. Each envelope is defined by four attributes of air that surrounds the IT equipment: Dry bulb temperature, Humidity Ratio, Relative Humidity and Saturation Temperature. It should be noted that the temperature range specified is for inlet air conditions. The wide range of classes A3 and A4 allows the application of free-cooling methods. However, the use of free cooling at high outdoor temperatures can be critical due to the enhanced noise level and energy consumption of the fans. The type of IT equipment in this study is unknown, thus the limits of class A1 are applied. Those limits are within 18°C to 27°C dry-bulb temperature and within 20% to 60% relative humidity.

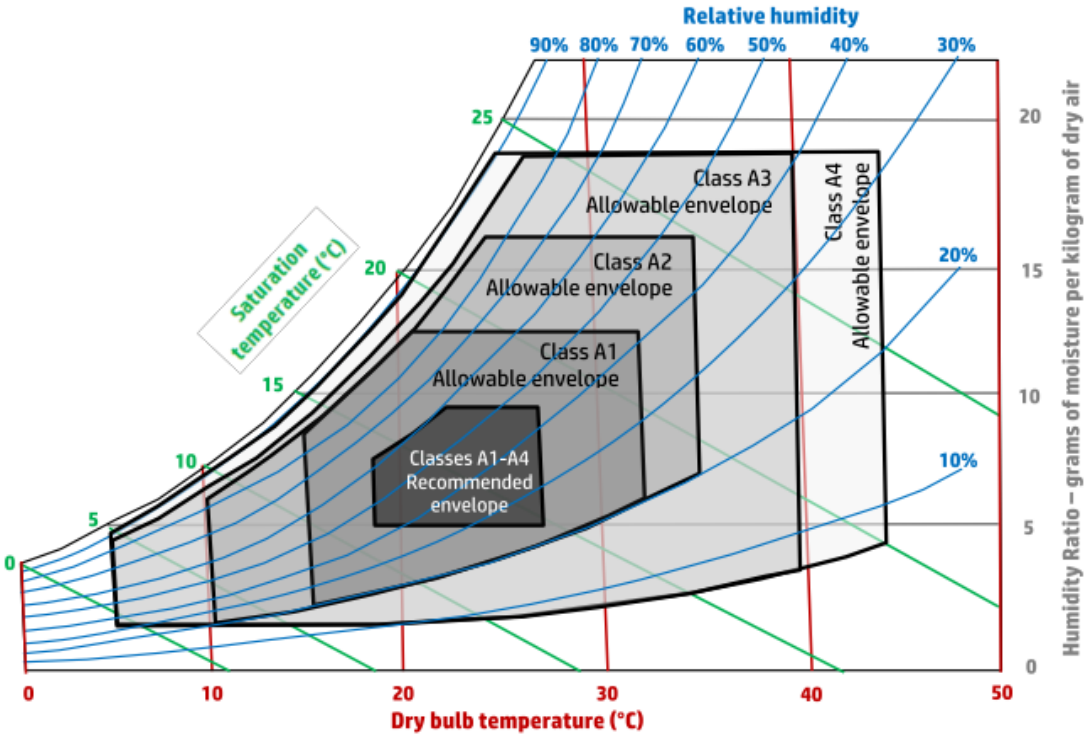

Figure 2-2: ASHRAE Thermal operation range for data centers [18]

2.3 Review of Cooling Techniques

As the power density in data centers increases every year, choosing the suitable cooling technique is critical. Having a reliable cooling system is crucial, since cooling system outages can cause temperature rises of up to 5°C per minute and reach disastrous levels [19], [20]. The following subchapter introduces the basic refrigeration cycle and specific heat removal methods for modular data centers.

Refrigeration Cycle

In a data center the electricity used to run the IT equipment is nearly 100% transformed into heat [16], [21]. Air conditioners use mechanical energy to pump the dissipated heat energy to the outdoors. Using the refrigeration cycle dissipated heat energy is moved from the data center room to the outside environment. Figure 2-3 represents the refrigeration cycle with its main components: evaporation, compression, condensation and expansion. The refrigerant is a substance that transports heat out of the data center.

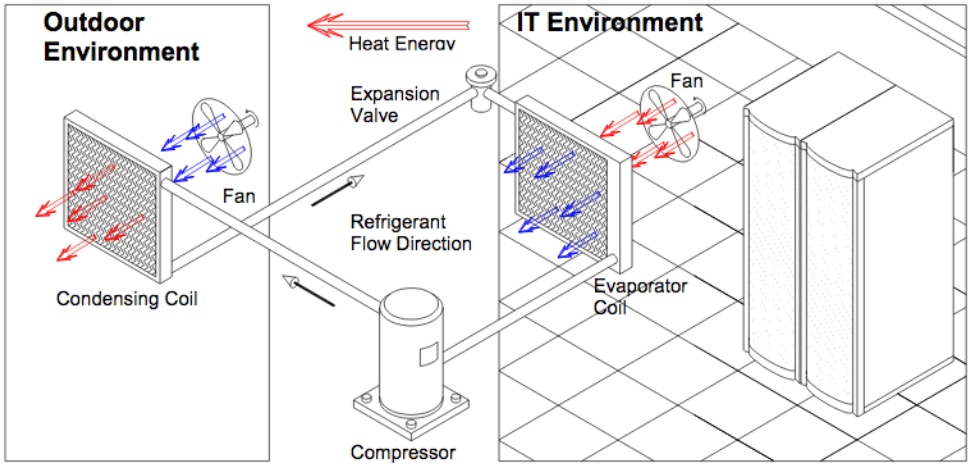

Figure 2-3: Refrigeration cycle in ICT facility covering interior and exterior environment [22]

In the first step, warm return air stream is blown across the evaporator coil by the fan and cooled down by the liquid refrigerant. That heat exchange leads to an evaporation of the refrigerant (at around 8°C). In a second step the evaporated refrigerant passes through the compressor and increases its pressure and temperature (above 50°C). Thus, it pushes the refrigerant to the outside environment where the condenser is located (where the temperature is cooler than the refrigerant temperature).
In the condenser heat is exchanged from the refrigerant to another medium (air, water), thus the refrigerant cools down and gets liquid again. Heat is exhausted to the outdoor.
In the fourth step the liquid refrigerant passes through the expansion valve, where pressure is reduced to a lower pressure. Pressure is regulated in order that the refrigerant can be fully evaporated in the evaporator again by the heat energy in the data center. The energy input for the entire process consists of the fan energy and the energy for running the compressor. Removing Heat from MCDs can be realized by the following specific cooling techniques. [23]

DX-Cooling (Direct Expansion)

The IT Equipment is air cooled inside the data center by using air-to-refrigerant heat exchangers. They are connected to air-cooled (or water-cooled) condensers located outside of the container. In fact, any system that uses refrigerant and an evaporator coil can be called a DX system. Packaged DX air conditioners are the most usual type of cooling equipment for smaller data centers. These systems are generally available as commercially equipment from manufacturers and described as CRAC (Computer Room Air Conditioner) units. Depending on the data center's climate zone and air management, a DX unit with airside economizer can be a very energy-efficient cooling option for a small data center.

Outside Air (Free Cooling with Economizer)

The IT Equipment is fully cooled by using "free" colder air from the outside that is pulled or pushed by a fan into the container. The mechanical device inside the HVAC system is called Economizer. It is a promising option to reduce energy consumption especially in colder climates.

Chilled Water System

The IT equipment is air-cooled by air-to-water heat exchangers. A chilled water plant equipped with water-cooled (or air-cooled) chillers produces the chilled water. Water-cooled chillers are typically located indoors. These systems are cost-expensive in terms of investment for small installations, however they are typically less energy consuming than DX systems.

In order to get an idea about the total efficiency of existing data centers and to be able to compare the performance among different data centers, two metrics in literature are utilized [24]:

- DCIE: Data Center Infrastructure Efficiency, which is the Total IT Power divided by Total Facility Power
- PUE: Power Usage Effectiveness, which is the Total Facility Power divided by Total IT Power (reciprocal of DCIE)

However both metrics give only information about efficiency relative to energy demand, but not about the resource impact such as carbon intensity or water utilization [1]. In order to get an overview about the relative performance between cooling types, the average PUE of different cooling systems based on vendor product characteristics are analyzed in literature [12]. The resulting plot is shown in Figure 2-4.

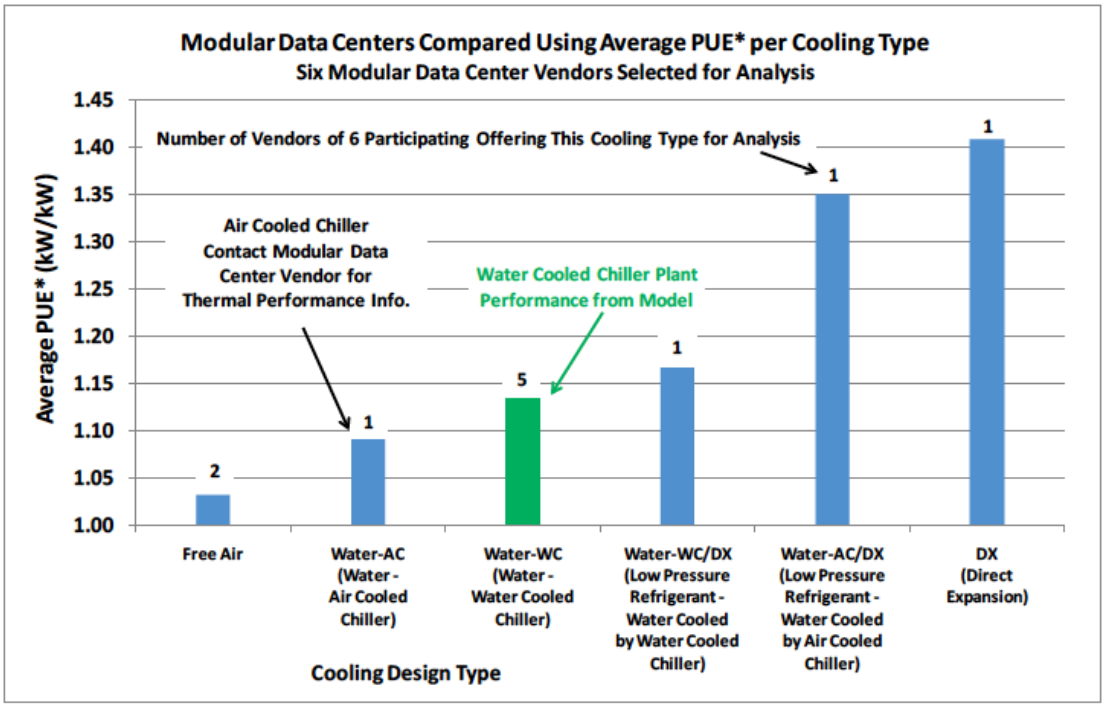

Figure 2-4: Comparison of PUE of different cooling techniques for MDCs [12]

Results show lowest PUE (less than 1.05) for free air-cooling while DX air-cooling appears to have highest PUE (1.40). Using “air-to-water” or “air-to-low pressure refrigerant” heat exchangers can increase overall efficiency.

Manufacturers of portable or modular data centers normally use Direct Expansion (DX) cooling to cool the equipment within their data center. Examples of these include Huawei and a few others [25]. Dell offers his MCDs with optional chilled water cooling in combination with free-air cooling [10]. New innovative developments are liquid-cooled systems by Asperitas [26]. These small (600 x 1200 mm) self-contained units contain oil-immersion that circulates by natural convection inside the IT equipment. Heat is rejected then by a common water source. Liquid cooling can operate higher heat densities as water flow is a much more efficient method of transporting heat than airflow.

2.4 Energy Management in Data Centers

Data center spaces can consume up to 200 times more electricity as regular office spaces. Thus, it is very important to implement intelligent and energy efficient design measures that can reduce costs and reduce energy consumption. This sub-chapter presents some common measures to reduce electricity use in data center environments [27], [28].

The energy to run IT Equipment can account for more than 50% of the facility's total consumption, if the cooling system is highly efficient. Consequently, efficient IT equipment can show a notable reduction of total consumption. As a result, cooling equipment could also be scaled down. IT servers that are equipped with energy-efficient processors, fans, power supplies and high-efficient network equipment are suitable to reduce IT equipment loads within a data center. Applying the following intelligent measures to the IT equipment set up can reduce energy consumption of HVAC equipment.

Intelligent air management in data centers can additionally reduce energy costs. Air stream configurations that eliminate mixing of both supply air stream and return air stream is an effective measure (hot aisle/cold aisle configuration). It minimizes exhaust heat going back into the IT equipment and bypass heat around the IT equipment. A possible configuration is an overhead heat return and an under-floor air distribution system. Consequently, operating costs decrease and data center's power density (W/m^2) increases [21].

Increasing the supply air temperature can help to reduce the size of the air-side cooling equipment required. Especially if lower-cost packaged air handling units are used. The lower required supply airflow due to raising the airside temperature delta gives the opportunity for fan energy savings [27].

Another intelligent measure is to use a variable air volume delivery cooling system for steadily providing cooling when and where it is needed. A control system should be implemented to maximize the energy efficiency of the cooling systems under variable ambient conditions as well as variable IT loads. Supply air and supply chilled water temperatures (in a water-cooled system) are most efficient when set as high as possible while keeping the necessary cooling capacity. Humidity in data centers is

typically over controlled. This results in increased energy use. Humidity control generally can be relaxed or shut down for many locations [27].

Direct liquid cooling of components offers great cooling system efficiency by removing airflows completely. Transferring heat from a small volume of warm air directly off the equipment to a chilled water loop is more efficient than removing heat from the entire mixed volume of room air. Thus, the direct liquid cooling method needs a rack that is strictly separated from the rest of the data center room in order to work effectively with a chilled water system [28].

If there are different time-sensitive tariffs, it is recommended to apply a demand response control to the IT equipment. If a demand response event takes place, an intelligent management system can reduce IT equipment loads or switch to backup power generation. As well it is possible to shut down IT equipment that idles [27].

Data centers produce a great amount of waste heat that can be used directly if possible. The direct use of waste heat for low temperature heating applications such as preheating ventilation air for buildings or heating water will provide global energy savings. This measure is limited due to the typically remote locations of modular data centers. In larger systems waste heat can be used to supply cooling required by the datacenter through the use of absorption or adsorption chillers [27].

The combination of a mostly steady electrical load and the requirement for reliable power supply make large datacenters well suited for on-site generation. To reduce costs, on-site generation equipment could replace the backup generator system. Another possibility is reducing the total operation costs by selling the surplus power back to the grid utility [27]..

2.5 Room Air Heat Transfer and Heat Balance Fundamentals

In this chapter, the fundamental heat transfer methods and room air heat balance affecting the thermal performance of modular data centers will be analyzed. This chapter serves as a theoretical basis for the development of the simulation models in sub-chapter 3.5.

The heat balance method takes the fundamental thermodynamics of a building envelope by applying the First Law of Thermodynamics (conservation of energy) to critical points within the building geometry. The heat balance approach applies a control volume at the outside face of every building surface, at the inside face of every building surface, and around the inside air of each thermal zone defined within the building. It is a suitable method to obtain the cooling requirements of a building model [29].

Outside Surface Heat Balance

In the outside surface heat balance, the four heat transfer mechanisms acting on the control volume at the outer surface of each wall as shown in Figure 2-5 must be balanced for energy to be conserved.

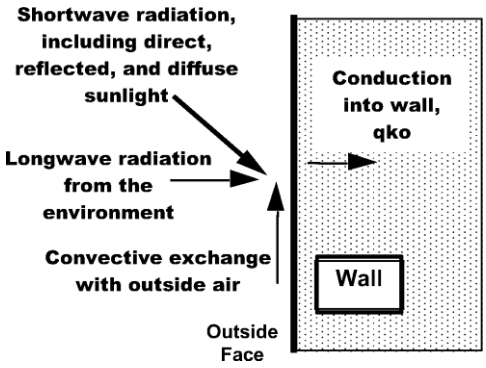

Figure 2-5: Outside Surface Heat Transfer with the boundary wall surface and outside [29]

The heat balance on the outside face of each surface is shown in equation (2.1):

$$q''_{\propto sol} + q''_{LWR} + q''_{conv} - q''_{ko} = 0 \qquad \textbf{(2.1)}$$

with:

$q''_{\propto sol}$	= Absorbed direct and diffuse (short wavelength) radiation heat flux	[W/m2]
q''_{LWR}	= Net long wavelength (thermal) radiation flux exchange with air, surroundings	[W/m2]
q''_{conv}	= Convective flux exchange with outside air	[W/m2]
q''_{ko}	= Conduction heat flux (q/A) into the wall	[W/m2]

Inside Surface Heat Balance

In the inside surface heat balance, the six heat transfer mechanisms acting on the control volume at the inside surface of each wall, as printed in Figure 2-6, must be balanced for energy to be conserved.

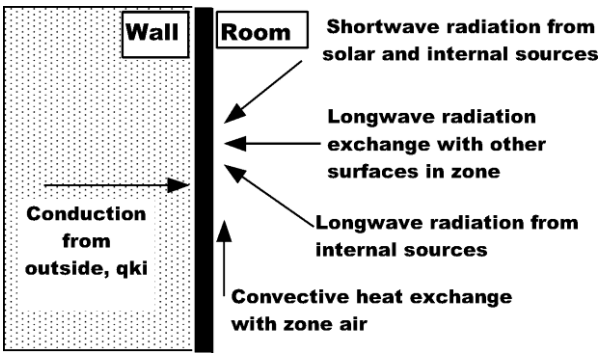

Figure 2-6: Inside Surface Heat Transfer with the boundary wall surface and room [29]

The heat balance on the inside face of each surface is shown in equation (2.2):

$$q''_{LWX} + q''_{SW} + q''_{LWS} + q''_{ki} + q''_{sol} + q''_{conv} = 0 \quad \textbf{(2.2)}$$

With:

q''_{LWX}	= Net longwave radiant exchange flux between zone surfaces	[W/m2]
q''_{SW}	= Net short-wave radiation flux to surface from lights	[W/m2]
q''_{LWS}	= Longwave radiation flux from equipment in zone	[W/m2]
q''_{ki}	= Conduction flux through the wall	[W/m2]
q''_{sol}	= Transmitted solar radiation flux absorbed at surface	[W/m2]
q''_{conv}	= Convective heat flux to zone air	[W/m2]

Zone Air Heat Balance

The zone air heat balance allows to estimate the zone-cooling load respectively the corresponding zone air temperature. The fundamental assumption of heat balance models is that air in each thermal zone can be modeled as well mixed with a uniform temperature. The heat balance on the room zone air is shown in equation (2.3).

$$C\frac{dT}{dt} = \dot{Q}_{convGains} + \dot{Q}_{convSurfaces} + \dot{Q}_{Inf} + \dot{Q}_{Sys} \quad \textbf{(2.3)}$$

With:

$C\frac{dT}{dt}$	= Energy stored in zone air	[W]
$\dot{Q}_{convLoads}$	= Convective internal gains	[W]
$\dot{Q}_{convSurfaces}$	= Convective heat transfer from zone surfaces	[W]
$\dot{Q}_{Inf}$	= Heat transfer due to Infiltration of outside air through cracks	[W]
$\dot{Q}_{Sys}$	= Air systems output (HVAC)	[W]

While a solution can be found for this system of equations, the solution process generally involves either an iterative method or a more complex solution algorithm that can be established with the aid of simulation software. To solve the heat balances for thermal zones, the three mechanisms of heat transfer (conduction, convection and radiation) through surfaces are considered. The incident solar radiation on the exterior surfaces is partially reflected to the environment and the other part is conducted into the surfaces, where it is stored and transferred into the interior surface. In the inside face heat is transferred by convection and radiation to/from the room.

Conduction

Thermal conduction is the process of heat transfer from one part of body (here wall) at a higher temperature to another at a lower temperature. Heat can be conducted through solids, liquids and gases without movement of molecules. The equation for conduction is (2.4):

$$\dot{Q} = k\,A\,\frac{T_{hot} - T_{cold}}{L} \quad \textbf{(2.4)}$$

With:

k	= Thermal conductivity of the material	[W/mK]
A	= Surface Area	[m^2]
T_{hot}	= Hot Surface Temperature	[K]
T_{cold}	= Cold Surface Temperature	[K]
L	= Thickness of the wall	[m]

Convection

Heat transfer from one location to the next by the movement of fluids is called convection. The fluid flows from a hot temperature location to a low temperature location. The moving fluid carries energy with it. Heat transfer from surface convection is calculated using the established equation (2.5):

$$\dot{Q} = h\,A\,(T_{surface} - T_{air}) \quad \textbf{(2.5)}$$

With:

h	= Exterior/Interior convection coefficient	[W/m^{2}K]
A	= Surface area	[m^2]
$T_{surface}$	= Surface temperature	[K]
T_{air}	= Air temperature	[K]

Radiation

The building envelope exchanges heat by radiation. When two or more bodies at different temperatures exchange heat by radiation, heat will be emitted, absorbed and reflected by each body. The radiation heat exchange between an exterior surface and the sky with a “grey body” ($\varepsilon \neq 1$) the Stefan-Boltzmann Law can be expressed as equation (2.6):

$$\dot{Q} = \varepsilon\,\sigma\,F_{air}\,A\,(T_{sky}^4 - T_{surface}^4) \quad \textbf{(2.6)}$$

With:

ε	= Emissivity of the surface	[-]
σ	= Stefan-Boltzmann constant	[W/m^2·K^4]
A	= Area of the surface	[m^2]
F_{air}	= View Factor of Surface to Air Temperature	[-]
T_{sky}	= Air Temperature	[K]
$T_{surface}$	= Surface Temperature	[K]

Radiation exchange occurs furthermore with the ground, the air (exterior) and other surfaces (interior).

3 Development of Thermal Models

The first part of this chapter characterizes the four different facilities that are the subjects for the development of the thermal simulation models of containerized data centers. The approach is general and could also be applicated on other facilities or locations. The methods of treatment of climatic and facility data are also reviewed in the first part of the chapter. The design and the limitations of the simulation models are discussed in detail throughout the remaining part of the chapter. Furthermore, the corresponding simulation software is presented comprehensively. The development of simulation models in this chapter is the foundation for the objectives of thermal model calibration and optimization further on in this study.

3.1 Characterization of the ICT Facilities

This sub-chapter describes the four facilities regarding their location, geometry, equipment and sensors. These given parameters are fundamental requirements for the model design in the remaining part of chapter 3.5.

3.1.1 Location

The four MDCs are in Portugal mainland and are distributed around the following places: Montalegre, Cinfães, Salvaterra de Magos and Mourão. The geographic allocation is presented on a map in Figure 3-1.

Figure 3-1: Facilities location distribution throughout Portugal [30]

3.1.2 Geometry

This study analyzes two different geometries of MCDs: the large container size is used in Cinfães and Salvaterra de Magos; and the small size is used in Montalegre and Mourão. The photos in Figure 3-2 show the two different geometries.

Figure 3-2: Data center geometries: large 20 ft. container (left) and small 10 ft. container (right)

The exact dimensions are assumptions of the author and built on standard references for 10 ft. respectively 20 ft. containers [31]. The measurements are presented in Table 3-1.

Table 3-1: Dimensions of the large and small containers.

Location	Dimensions [mm] length x width x height
Cinfães	6058 x 2438 x 2591
Salvaterra de Magos	
Montalegre	3029 x 2438 x 2591
Mourão	

The containers are placed slightly elevated on a concrete pad to avoid direct ground contact. Doors are positioned on the front side of the containers. HVAC equipment is mounted on the backside walls. Colors of the container envelopes are white/grey to keep the absorptivity as low as possible.

3.1.3 Cooling Equipment

The cooling equipment specifications are described in Table 3-2. The cooling equipment of a large container consists of two DX PTAC (Packaged Terminal Air Conditioner) units, each with 6.36 kW total

cooling power. In contrast, a small container is equipped with only one PTAC unit with 6.36 kW and an additional Split unit of 5 kW. The cooling units are mounted on the exterior walls, as shown in Figure 3-3. A Split unit is locally separated between the interior and the exterior. Thus, only the evaporator is mounted inside (ceiling) and is connected with pipes to the outdoor unit (condenser). In both systems, the condensers are cooled by outside air. The PTAC units are equipped with damper and fans that allow free air-cooling of the conditioned space. Depending on the temperature of the outside air, mechanical cooling can be switched off completely or partly (0 to 100%).

Table 3-2: Cooling Equipment Specifications

Feature	Large Container	Small Container	
Cooling Units	2 x Climaveneta MED 0021	1 x Climaveneta MED 0021	1 x Toshiba RAV-SM563AT-E RAV-SM564CT-E
Total Cooling Power	2 x 6.36 kW	1 x 6.36 kW	1 x 5.00 kW
Sensible Heat Ratio	0.89	0.89	0.7
Calculated COP	3.63	3.63	2.75
Compressor Power	2x 1.62 kW	1.62 kW	1.82 kW
Evaporator Fan Power	2 x 0.26 kW	0.26 kW	
Max Air Flow Evaporator Fan	1450 m^3/h	1450 m^3/h	780 m^3/h
Cooling Type	DX-Air PTAC	DX-Air PTAC	DX-Air Split System
Refrigerant	R410A	R410A	R410A
Free Cooling	Yes	Yes	No

It can be assumed that the split systems are additional units used to increase total cooling capacity for the small containers, if necessary. Furthermore, the maximum COP (Coefficient of Performance) of the split systems (2.75) is lower than the PTAC units (3.63). The COP is calculated as gross cooling power capacity divided by electrical power input (compressor and condenser fan power). Still, the actual COP is varying depending on the environment conditions. The PTAC units have a sensible heat ratio (sensible capacity divided by gross cooling power capacity) of 0.89, as MDCs typically have low moisture removal.

Figure 3-3: Cooling units: large container setup with 2 x PTAC units (left), small container setup with 1 x PTAC and 1 x Split unit (right)

Figure 3-4: Interior supply and return air openings of the PTAC units

As shown in Figure 3-4, the air supply in the PTAC case comes from the top open, while the bottom open receives the return air. A display terminal is ready to configure temperature and additional set points.

3.1.4 Sensors

The containers have two principal output parameters: energy consumption and air temperature. These parameters are being measured by different sensors that have been placed inside the container and feed the measured data to an online platform. Four sensors measure the air temperature at various locations:

- T1: measures indoor air temperature
- T2: measures outside supply air (free-cooling)
- A3: measures indoor air temperature
- ESP8266: measures indoor air temperature

The exact position and difference of the indoor air temperature sensors in the container is unknown. The energy consumption is measured by a wattmeter in each container. Those that are installed in the small containers have a time-step of 1 measurement per hour, while the ones that monitor the large containers have a time-step of 60 measurements per hour (1 per minute).

3.2 Facility Energy and Temperature Data

The electricity and temperature data are extracted from an online platform that is gathering all data in a CSV file format[1]. Facility data processing is a preparation for the model development. The objective is not to complete the datasets, rather to make the available data usable. For visualizing hourly simulation output, the software DView is used in the manual calibration [32]. As the plotting software only accepts input files with 8760-hour values, it must be ensured that missing hours are identified and included in the dataset.

There are four temperature sensor datasets available: T1, T2, A3, ESP8266. As sensor T2 measures outdoor air, it is not treated further. The other three sensors are imported in Excel PivotTable that allows to sort values by month/day/hour to identify data gaps. Furthermore, it permits to make hourly averages of 1-minute values (in the case of ESP8266). If only one hourly value is missing, the average of the hour before and after is used. If successive values are not available, the values are set to zero. Only sensor T1 is used as reference sensors in the further process of this study, as it has the fewest data gaps.

Electricity data is measured by a wattmeter in each facility. Cinfães and Salvaterra de Magos produce 1-minute values that are averaged to hourly values, while Montalegre and Mourão produce hourly values. To identify data gaps, Excel PivotTable is used again. Particular and successive hourly data gaps are set to zero, as it is important to generate an input file with 8760 values. It allows to compare measurement with simulation data in DView in the model calibration.

The general time period of available data (with gaps) for Cinfães is March to December 2016, while for Salvaterra de Magos only December 2016 to March 2017. For the small containers data is available from May to December 2016.

3.3 Modeling Software

This subchapter gives an overview of the different software tools that are used to create the simulation model. To facilitate the building process with EnergyPlus, two additional programs are used to create the geometry (SketchUp) and to create the weather file (Elements). The workflow is visualized in Figure 3-5.

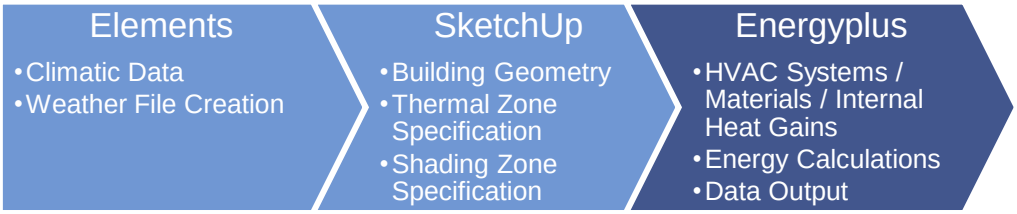

Figure 3-5: Workflow of Model Design

[1] This online platform has been developed by an energy efficiency company, Watt-is (www.watt-is.com)

3.3.1 EnergyPlus

EnergyPlus is one of the most used programs in the field of building energy simulation [33]. It is used as the main analysis tool in various research papers addressing a broad range of problems related with energy and environmental performance of buildings. EnergyPlus allows handling both the input data and the simulation results through comma-separated value (CSV) files that eases the integration to other (visualization) programs. The entire model specifications are contained in an input data file (IDF). The modeling workflow starts with creating the geometry using SketchUp. Then, EnergyPlus native, or any third-party software such as OpenStudio, can then be used to define the model's system specifications. In this study EnergyPlus version 8.4.0 is used.

3.3.2 SketchUp

The Legacy OpenStudio Plug-in for SketchUp is a useful tool to create the building geometry for the EnergyPlus input files. The Legacy plug-in (Version 1.0.14) is released within SketchUp 8. This makes it possible to draw a 3D-Model and convert the geometric points automatically in an arranged EnergyPlus input file. The Plug-In reads and opens every EnergyPlus Input file (IDF), if corrections in the geometry are necessary in a posterior project phase. Thermal and shading zones can already be determined within the software. The application of SketchUp is described further within the sub-chapter 3.5.1.
The Legacy OpenStudio Plug-in was created by the National Renewable Energy Laboratory for the U.S. Department of Energy as an interface to the EnergyPlus simulation engine [34]. Recent development has moved from the Legacy OpenStudio Plug-in to the more complete OpenStudio suite of tools and as a graphical user interface for EnergyPlus. Changes to the Legacy OpenStudio Plug-in will be limited to bug fixes and compatibility updates for new versions of EnergyPlus.

3.3.3 Elements

Elements, Version 1.0.6, is a program that is developed to create or modify existing weather files (EPW) for EnergyPlus [35]. The open-source tool allows editing temperature, radiation, wind speed or humidity values. Furthermore, it is possible to scale or normalize certain variables by monthly average or monthly minimum/maximum. Big Ladder Software developed Elements software tool with the funding and collaboration of Rocky Mountain Institute. The application of Elements is described further within the sub-chapter 3.4.

3.4 Climate and Weather Data Treatment

The climatic and weather data treatment for the four case study locations is described in this sub-chapter. The creation of weather files is an essential step before starting with the EnergyPlus model.

Since the thermal model needs to be calibrated on the facility's measured data from the years 2016 and 2017, the weather data must correspond to same time period.

3.4.1 Weather File

The EnergyPlus weather file contains various information such as data on latitude/longitude, elevation and as well as on the following climatic parameters: dry bulb temperature, wet bulb temperature, dew point temperature, relative humidity, atmospheric pressure, wind speed, global solar irradiance, normal solar irradiance and diffuse solar irradiance.
The weather files that are used for the four locations in this study are modifications of existing TMY (Typical Meteorological Year) weather files that are generated with the Excel based software CLIMAS-SCE [36]. A TMY is a data set of hourly values of selected weather data for a 1-year period (8760 hours) averaged over various years. LNEG developed this database and provides the climatic and meteorological reference data for various locations within Portugal. The TMY weather files are imported and then modified in Elements Software as explained in the sub-chapter 3.4.2.
Since TMYs provide average values over past several years, instead of recent data for a given year, the use of TMYs is not appropriate for thermal models that need to be calibrated the most precisely as possible. Thus, the available weather files are corrected to obtain files with hourly values of the climatic parameters for the year 2016 and 2017, respectively. Also, if the recent reference values are not exactly from the facility locations, it is more appropriate for calibration than TMYs. Salvaterra de Magos provides electricity consumption data from December 2016 to March 2017 and the remaining locations from March or May to December 2016.

3.4.2 Temperature, Humidity and Wind Speed

There are some limited sources available for free of charge and hourly measured weather data. The temperature, atmospheric pressure and wind speed data is acquired from the NNDC Climate Data [37] that provide hourly measurements of various weather stations within Portugal. Humidity is derived from the dew point temperature. Due to proximity to the case study locations and data completeness the following stations are chosen:

- Villa Real (for Cinfães and Montalegre)
- Montijo (for Salvaterra de Magos)
- Beja (for Mourão)

The TMY values are replaced by the NDCC values for temperature and wind speed of 2016 respectively 2017. As the weather stations are as far as 100 km away from the case study containers, the NDCC temperature values are scaled based on monthly min/max temperatures in Elements Software to achieve more precise results in a next step. Meteoblue [38] provides simulated plots of

monthly min/max temperature profiles for each case study location. The maximum and minimum temperatures are extracted from the plots for each month as shown in the example for Cinfães in Figure 3-6.

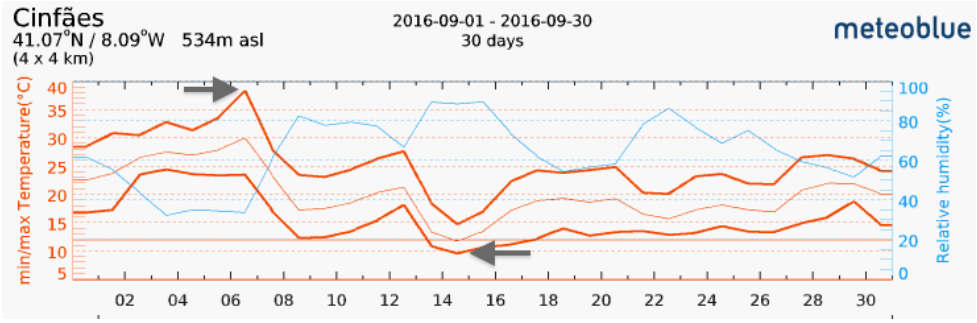

Figure 3-6: Monthly min/max temperature plot of a case study location to extract the monthly temperature minima and maxima

Elements Software provides a scaling option by monthly minimum and maximum temperature. Thus, the minima/maxima obtained with NNDC Climate Data are replaced with the minima/maxima of Meteoblue, as shown in the example in Figure 3-7. Subsequently Elements Software scales all hourly temperatures according to the new minima/maxima values.

Normalize By Month ×

Target Variable: Dry Bulb Temperature

Variables to Hold Constant: Relative Humidity, Atmospheric Pressure

Scaling Method: Scale by Minimum/Maximum

Month Year	Current Min [C]	Current Max [C]	New Min [C]	New Max [C]
January 2016	0.60	17.20	0.60	17.20
February 2016	-1.10	13.90	-1.10	13.90
March 2016	0.60	17.80	0.60	17.80

Figure 3-7: Elements Software; Example of Hourly Temperature scaling by monthly Minimum/Maximum

3.4.3 Solar Radiation

The solar radiation data is obtained from CAMS radiation service [39], which provides hourly values from 2004 up to 2 days ago. Incoming shortwave radiation consists of three components. Global Horizontal Irradiance (GHI) is the total amount of shortwave radiation received from above by a surface horizontal to the ground. This value includes both Direct Normal Irradiance (DNI) and Diffuse Horizontal Irradiance (DHI). The corresponding calculation is calculated using equation (3.1):

$$GHI = DNI \cdot \cos\theta + DHI \quad \textbf{(3.1)}$$

With:

θ = Solar Zenith Angle

The solar zenith angle is the incident angle of the sun's rays to the surface. The zenith angle is left unchanged from the TMY reference file.

3.5 Thermal Models

The design of the simulation models is described in this sub-chapter. The geometry is drawn in SketchUp, while the major part of the model is made in EnergyPlus. This includes for instance the definition of the materials, HVAC system and electrical equipment. However, this chapter describes the design phase of the base frame of the simulation models to keep the model running, while a few parameters are still adjusted in the calibration phase.

3.5.1 3D-Geometry

The geometry of the given sizes in chapter 3.1.2 is created using SketchUp. The container envelope is implemented in one thermal zone that is also created within SketchUp. The geometries (large and small) are shown in Figure 3-8 below. The containers have a floor area of 14.78 m^2 and 7.39 m^2 respectively. Both models are designed with doors (2.10 x 0.96 m). The geometries are automatically converted into EnergyPlus Input files for further settings.

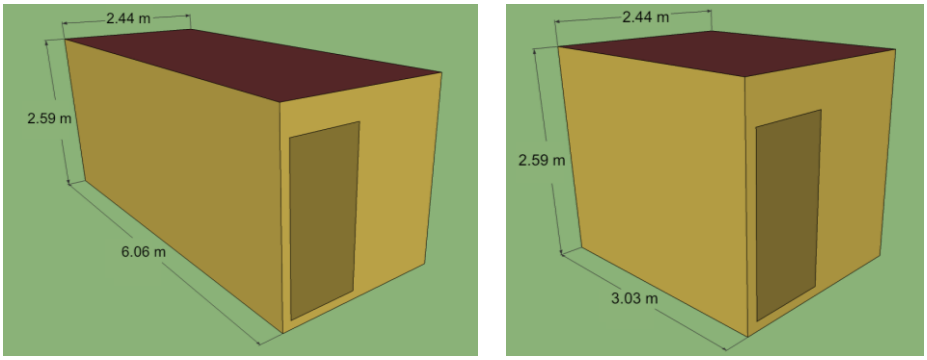

Figure 3-8: 3D-Geometry of large (left) and small (right) container models in SketchUp

3.5.2 General Simulation Settings

The boundary conditions for the simulation models are described in the following. The heat transfer algorithm outside is DOE-2 [40], which uses a correlation for the convection coefficient from measurements for rough surfaces. The inside heat transfer algorithm is TARP [41] that is calculated for natural convection based on temperature difference. The number of simulation time steps is 6 per hour. Before the actual simulation starts, EnergyPlus performs an automatic sizing of the HVAC system based on the design day of the weather file to determine the design cooling flow rates and loads.

3.5.3 Construction Materials and Insulation

The insulation level determines the heat transmission through the building wall and is defined by the selection of building materials. It is calculated with the total thermal resistance, R_T, of all external constructions, which in this case correspond to walls, roofs and external floors. The thermal resistance R_j of each material layer is defined by the equation (3.2):

$$R_j = \frac{d}{\lambda} \quad \textbf{(3.2)}$$

The resistance is derived from the thickness *d* (m) and thermal conductivity of the material λ (W/(m K))). The total resistance R_T is then expressed by equation (3.3):

$$R_T = R_{internal} + R_j + R_{external} \quad \textbf{(3.3)}$$

EnergyPlus calculates the inverse of the total resistance, the U-Value (W/(m^2 K)), by using the internal surface resistance $R_{internal}$, external surface resistance $R_{external}$ and material resistances R_i. Derived from that, the tptaç resistance for the container walls is 0.65 ((m^2 K)/W) estimated in EnergyPlus based on the wall materials. This is a low value compared to average R-Values for walls in Portugal of 2 ((m^2 K)/W) [42]. An overview of the materials is printed in Table 3-3. Surface materials are referenced on the Rittal Data Center Container [43]. The specifications of the insulation are based on cellular glass [44], while the insulation thickness results from the manual calibration in chapter 4.1. Moreover, this value is chosen assuming that the containers have small insulation thickness.

Table 3-3: Surface Materials and Resistances

Surface	Material	Density [kg/m^3]	Spec. Heat [kJ/m^{2}K]	Thick-ness [m]	Con-ductivity [W/mK]	Total* Resistance [m^{2}K/W]	U-Value* [W/m^{2}K]
Walls / Door	Metal	7824	0.5	0.002	45.28	0.65	1.54
	Insulation	115	1.0	0.02	0.04		
Roof	Metal	7824	0.5	0.003	45.28	0.64	1.57
	Insulation	115	1.0	0.02	0.04		
Floor	Metal	7824	0.5	0.002	45.28	0.69	1.45
	Insulation	115	1.0	0.02	0.04		
	Metal	7824	0.5	0.004	45.28		

*Include interior and exterior convective surface resistances

The containers are painted in a light color to avoid the absorption of solar radiation. The solar absorption indicates the amount of radiant energy of the total incident solar radiation that is absorbed by a color. In this thesis the solar absorption is set to 0.4 [45].

3.5.4 Thermal Mass

Building materials with higher thermal mass (denser and with higher specific heat capacity), such as concrete, brick and stone, have a greater ability to absorb daytime heat gains (reducing the cooling load and helping to avoid summer overheating). In turn, they release that heat during the night (reducing the heating demand), which can make the internal temperature of a building more stable. In contrast, buildings with low thermal mass (less dense or thin material layer) heat up quickly and the inside temperature follows in practice the daily external temperature profile if the internal heat gains are constant.

In data centers, the thermal mass of steel racks can eventually be meaningful to slow down overheating during HVAC shutdowns. If the server CPU power increases, the cooling power can be increased slowly to the desired higher level, rather than ramping up abruptly [25].

Defining thermal mass of the container envelope is possible with the global heat capacity C_G (kJ/m²K), which is also called Thermal Mass Parameter (TMP) as described in ISO 13790:2008 [46]. The corresponding equation is printed in (3.4):

$$C_G = \frac{\sum \kappa_i \cdot A_i}{A_{Floor}} \quad \textbf{(3.4)}$$

With

κ_i	= Kappa value - heat capacity per square meter of each building surface	[kJ/m²K]
A_i	= Surface Area	[m²]
A_{Floor}	= Floor Area	[m²]

The surfaces i to be included are all external: walls, floors and roofs. Equation (3.5) represents the heat capacity per unit area κ (kappa value) and is a measure of the thermal response characteristics of the construction. The higher the value, the more heat will be stored for later release.

$$\kappa_i = \sum \rho_j \, c_j \, d_j \quad \textbf{(3.5)}$$

The calculation is over all layers j in the element and is the sum of the product of density ρ_j (kg/m³), specific heat capacity c_j (kJ/kgK) and material thickness d_j (m). The calculation starts at the inside surface and stops at whichever of the following conditions is encountered first:

- The total thickness of the layers exceeds 100mm
- The midpoint of the construction is reached
- An insulation layer is reached

In the case of the MDCs in this study, only the floors contain thermal mass. With the use of the floor material properties of sub-chapter 3.5.3, the global heat capacity of the containers results 15.83 kJ/(m^2K). Ideally a building should excess a value of 200 kJ/(m^2 K) in order to reach medium thermal mass construction [47]. Thus, it may be noticed that the containers construction has a very low thermal mass performance and the cooling load profile follows the daily external temperature profile as the internal heat gains are constant. This high influence of temperature in consumption justifies the importance of having accurate weather files. Hereupon, the internal mass of the servers and a possible internal temperature delay is not considered in this simulation.

3.5.5 Internal Gains

The internal gains in this study are only composed of the ICT equipment, which is assumed to be a constant load over time. The value for equipment base load is developed iteratively. The baseline total energy consumption (least amount of cooling) is supposed to be at night in a winter month. After a visual analysis of the different load profiles, a start value of 20% for cooling power of the total energy consumption is assumed and iteratively decreased throughout the calibration. The difference of total energy and cooling energy equals the ICT equipment power. The preliminary value of 5200 W equipment power for the large containers is derived iteratively in the manual calibration in chapter 4.1.2. The small containers are assumed to have 1500 W (Mourão) and 1100 W (Montalegre) equipment power respectively. The radiant and convective split was assumed to be 20% and 80% [48]. The convective part of the heat transferred from the equipment to the surroundings is an instantaneous load, because it is added to the room air without a time delay. The radiative part is absorbed by the walls and surfaces of the room and then dissipated over time. Internal gains by lights are neglected, as there is no occupation of the containers.

3.5.6 Infiltration Rate

Building infiltration or exfiltration (unwanted air that leaks into or from the building) generally depends on building features, such as height, exposition, HVAC operation and envelope leakage, as well as weather conditions (wind speed, temperature). Regarding the building envelope, the opening of doors or windows mostly triggers infiltration. In addition, cracks in the envelope as well as the porosity of constructions can cause infiltration. Thus, a negative indoor air pressure (when the inside pressure is less than the outside pressure) causes infiltration, while positive indoor air pressure causes exfiltration. HVAC systems tend to slightly positively pressurize the building by supplying more fresh air than exhausting old air.

Exfiltration can have a significant impact on the energy performance of office buildings, especially on heating demands in wintertime. Considering winter weather conditions in Portugal, exfiltration can be beneficially to decrease cooling energy in data centers. Due to this fact, it could be important to consider the effect of this variable on the environmental and energy performance of data centers.

However, it is important to observe that Infiltration rates are highly uncertain, thus a common strategy used in EnergyPlus is to assume fixed infiltration rates, sometimes using a different constant value depending on whether the HVAC system is on or off. Still, this strategy does not reproduce known dependencies of infiltration on outdoor weather and the complexities of HVAC system operation [49].
The value for the infiltration rate for all containers in the design phase has been set to 0.5 ACH (Air Changes per Hour) as recommended by CIBSE Guide A4-13 for air-conditioned buildings with moderately tight building envelope [50]. This value is constant over simulation time, as the HVAC system remains always active.

3.5.7 HVAC System

The HVAC system is chosen based on a unitary DX system without ducts. A DX air-cooling system comprises of a vapor compression refrigeration cycle with an air-cooled condenser. Thus a "HVACTemplate:System:UnitarySystem" object serves as the cooling unit in EnergyPlus. The airflow loop for a single zone is schematically represented in Figure 3-9.
Since EnergyPlus is limited to one HVAC unit per thermal zone, the two identical PTAC units are modeled as one large unit in the case of the large containers. The small containers are modeled without the additional Split system in the manual calibration in EnergyPlus. The cooling coil COP is fixed on 3.63 based on actual system's specifications of Table 3-2. The DX cooling coil rated power and sensible heat ratio were set to be auto sized on the warmest day of the year (design day). This allows the software to calculate their value based on the space cooling set points and design supply air temperature to meet the zone cooling load. As the supply design airflow rate is fixed for the large and small containers to 0.810 m^3/s and 0.405 m^3/s according to the real system specifications, it occurs that the auto-sized values of the cooling coil capacity and SHR are slightly different to the real values in Table 3-2. However, EnergyPlus simulates a maximum supply airflow rate at the design day of less than 0.70 m^3/s and 0.25 m^3/s, thus the cooling load is met at every time step, while the cooling coils are always running. The temperature set points 21°C and 23°C are defined based on the average indoor temperatures measured by sensor T1 for each location.
Heating coils are switched off since there is no heating needs through over the year. It is possible to model an additional air side economizer with an optional outdoor air inlet. This so called "free cooling" allows outdoor air to cool the interior container equipment, while mechanical cooling is switched off or reduced.

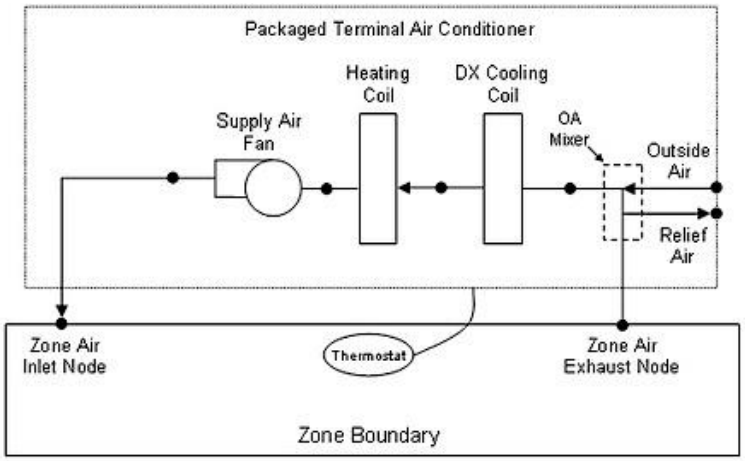

Figure 3-9: HVAC airflow loop in EnergyPlus [29]

Fan specifications are calculated with the EnergyPlus Fan Energy Calculator [51]. The system specifications are summarized in Table 3-4.

Table 3-4: HVAC specifications in EnergyPlus

Object	Specifications Large Container	Specifications Small Container
Cooling Set Point	21°C	23°C
Cooling Coil Type	Single speed DX	Single speed DX
Cooling Coil COP	3.63	3.63
Cooling Coil Design Capacity	13.41 kW (auto sized)	6.71 kW (auto sized)
SHR	0.80 (auto sized)	0.80 (auto sized)
Design Supply Air Temperature	14°C	14°C
Supply Fan Type	Cycling on/off, draw through	Cycling on/off, draw through
Supply Fan Delta Pressure	444 Pa	444 Pa
Supply Fan Total Efficiency	0.70	0.70
Supply Air Design Flow Rate	0.810 m^3/s	0.405 m^3/s

4 Calibration

The calibration process in this study is a data driven calibration approach [52], where data-driven models are using the system behavior in order to predict the system properties. In detail, this is a two-stage method with a manual calibration based on an iterative subjective approach followed by an automated calibration based on a parametric and mathematical optimization approach. The automated calibration is then backed up with a sensitivity analysis to identify the impact of different model parameters. The following sub-chapters describe the methods and results of the calibration.

4.1 Manual Model Calibration

Manual model calibration approaches mostly rely on iterative pragmatic intervention by the modeler. It is based on users' experience and judgment. It includes "trial and error" approaches, which are based on an iterative manual tuning of the model input parameters. Input data is changed based on the users' knowledge about the building. Manual calibration corresponds thus to subjective approaches. Within the manual calibration methodologies, techniques based on graphical representations and comparative plots of the results are included [53].

When merging measured and simulated values, two overall sources of error exist: (i) measurement error that comes from the raw data and (ii) model error generated from the simulation process. In general, the sources of uncertainty and limitations in building energy models can be classified and applied to this study:

- Scenario uncertainty (climate conditions, occupancy)
- Physical uncertainty (building envelope and material properties, internal gains, HVAC systems operation and control settings)
- Model inadequacy (model assumption, simplification in the simulation model algorithm)
- Observation error (metered data accuracy, sensor accuracy)

The first category "scenario uncertainty" addresses the outdoor weather conditions and the building use. Typically, real weather data are used for creating "real" weather files to be applied in simulation. Incomplete or inaccurate weather data can cause uncertainties definition of the weather file. Similarly, uncertainties can affect the building use, which is set by schedules that express the building operation. The second category is related to the uncertainties in the building modeling: envelope thermo-physical properties, the building internal gains (ICT equipment), the HVAC definition and its operational and control settings. As there are only photos of the containers available, envelope properties are quite uncertain. The third category "model inadequacy" indicates uncertainties in the building model. Each building model is thus an approximation of a real building, created based on assumptions and simplifications. The last category refers to observation errors in the measured data. The data quality of

measurement of energy consumption used for calibrating the model can affect the accuracy of the results. Furthermore, the types and exact locations of temperature sensors are unknown. As temperature sensor T1 provides the fewest data gaps, it represents the reference sensor in this study.

4.1.1 Simulated Operative Container Temperature

As the ICT equipment power is assumed to be constant over time and the cooling loads are always met by the HVAC system in EnergyPlus, the simulated interior mean air temperature of the containers is also almost constant. Only a slight variance from the temperature set point is given due to the infiltration rate, which corresponds to a maximum value of temperature variation is less than 0.01°C per time step.
However, the measured temperature sensors show a different behavior. Clearly, the interior container temperature is varying over the day, mostly with peaks during the afternoon. Thus, there should be a correlation to the daily outdoor climate and the temperature sensors, which may sense a part radiant energy fraction as well. According to [54] most temperature sensors measure a temperature between the mean air temperature and the operative temperature, if the sensor is not enclosed behind a shield.

As referred, to simulate the actual temperature in the containers more precisely and consequently improve calibration results, the simulated operative temperature output is used for calibration. The standard operative temperature is calculated by EnergyPlus according to equation (4.1) as half of the mean air temperature and half of the mean radiant temperature:

$$T_{Operative} = 0.5 \cdot T_{MeanAir} + 0.5 \cdot T_{MeanRadiant} \quad \textbf{(4.1)}$$

The mean radiant temperature $T_{MeanRadiant}$ is a measure of the combined effect of the temperatures of the surfaces within a space. It is calculated in EnergyPlus based on an area-emissivity weighted average of all the surface temperatures in the zone, where emissivity corresponds to the thermal absorptance of the inside material layer of each surface.
According to ASHRAE [55] there can be a correlation between the radiant fraction in the operative temperature equation and the supply air velocity. The recommended values are shown in Table 4-1. Based on that correlation, it is assumed in this study that the radiant fraction varies over time in the operative temperature equation.

Table 4-1: Correlation between air velocity and radiant fraction for operative temperature equation [56]

Supply Air Velocity [m/s]	Radiant Fraction
< 0.2	0.5
0.2 – 0.6	0.4
0.6 – 0.1	0.3

As the air velocity is not measured or simulated, the following radiant fraction values are only assumed based on the size of the cooling load and adjusted according Table 4-1. Large cooling loads due to high summer outside temperatures (August) may lead to higher air velocities of supply air. In contrast, modest cooling loads (January) may cause rather low supply air velocities.

Therefore, the output variable of the operative temperature is customized in EnergyPlus. The EMS module (Energy Management System) in EnergyPlus allows to create custom output variables. In this case, the EMS takes the simulated values of $T_{MeanAir}$ and $T_{MeanRadiant}$ and calculates a custom operative temperature with the assumed radiant fractions in Table 4-2. The radiant values are based on the month of the year and are rather conservative, compared to the proposed values in Table 4-1.

Table 4-2: Radiant fractions used for custom operative temperature output in EnergyPlus

Months	Radiant Fraction
January, February, December	0.4
March, April, October, November	0.3
May, June	0.2
July, August	0.1

4.1.2 Results from Large Containers Manual Calibration

The large containers are in Salvaterra de Magos and Cinfães. Both containers may have a similar setup and thus a comparative ICT equipment load. The ICT equipment load is the most important parameter to define, because it determines the electrical consumption and the cooling load (heat dissipated from the servers). After some iteration, by changing other input parameters simultaneously (materials, temperature set points, etc.), the value for the internal gain is defined as 5200 W. The results of simulated hourly container temperature and total energy consumption for both locations are illustrated in Figure 4-1 and Figure 4-2, respectively. The simulated container temperature is the operative temperature and is compared with the measured temperature (sensor T1). The presented time periods have full data availability and are alike the ones in automated calibration in sub-chapter 4.2.

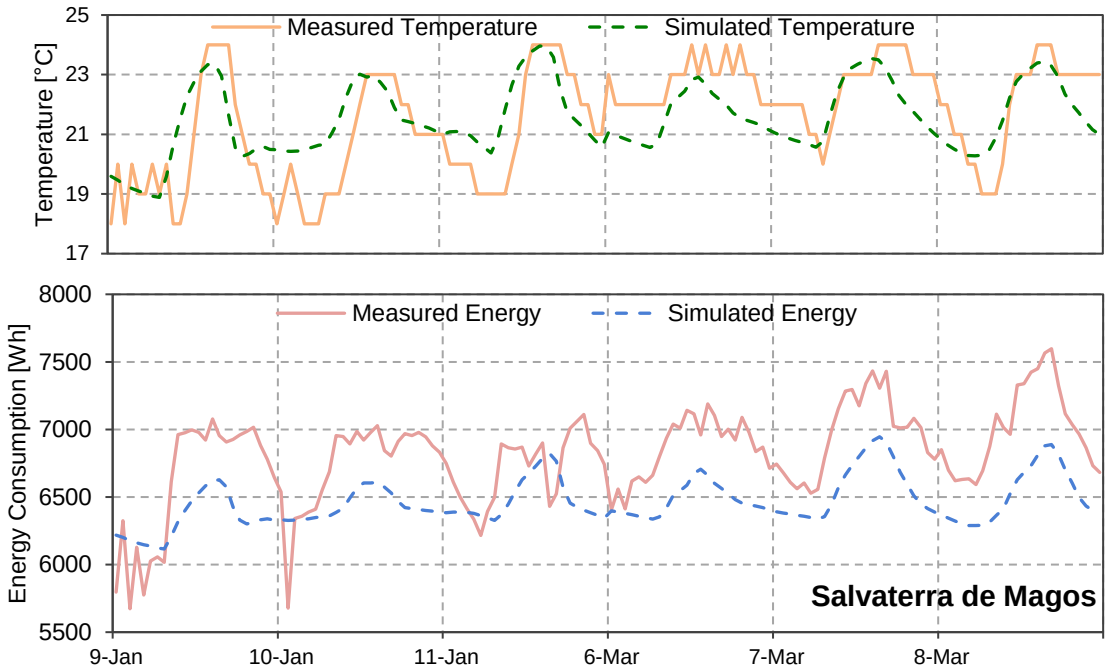

Figure 4-1: Manual calibration result for Salvaterra de Magos, comparison of simulated and measured temperature and energy consumption

To present two different time periods, a selection of three days each of January and March for Salvaterra de Magos is plotted. However, exterior climatic conditions should not vary too much for both months. As for the container temperature, a good fit of measurement and simulation is visible. In terms of energy consumption, the profile amplitude of measurement and simulation is already harmonizing, though there is still an offset of 1 kW visible. The simulated energy consumption should be underestimated and refined.

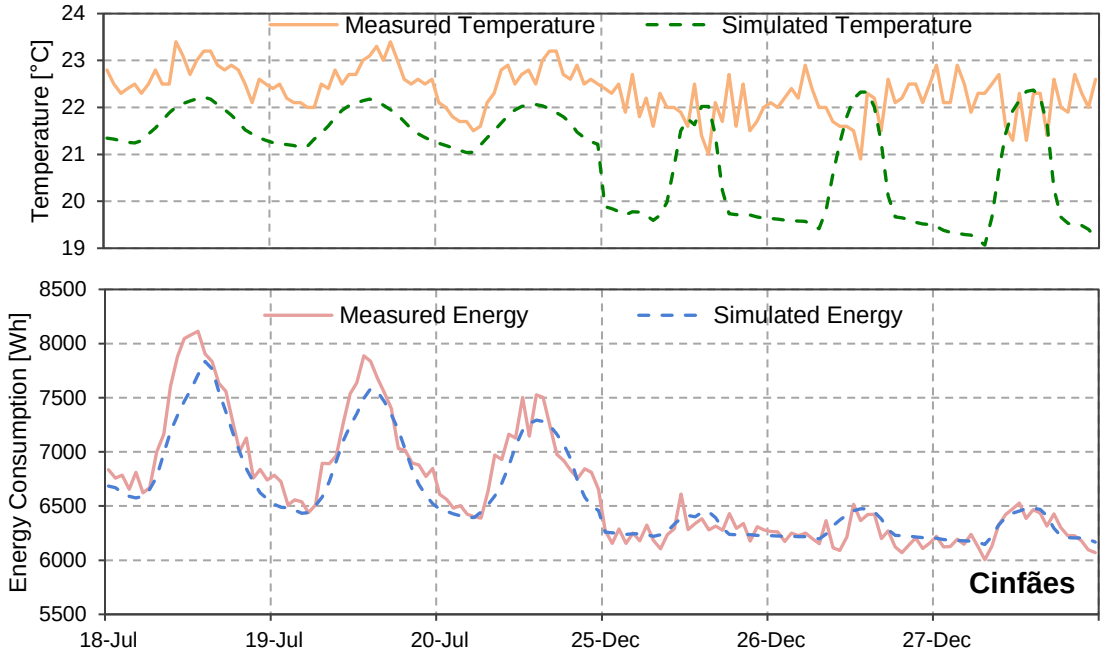

Figure 4-2: Manual calibration result for Cinfães, comparison of simulated and measured temperature and energy consumption

A selection of three days each of July and December is presented for Cinfães to identify the differences between summer and winter conditions. It can be noticed that temperature measurement and simulation profiles are similar in July, while in December discrepancies are identified. However, in both July and December there looks to be an offset, thus temperature set point in the simulation model could be adjusted in a next step in the automated calibration. Measured and simulated energy consumption profiles for Cinfães for both periods are most closely corresponding. Consequently, manual calibration is somewhat adequate.

4.1.3 Results for Small Containers Manual Calibration

The small containers in Mourão and Montalegre are equally manually calibrated regarding container temperature and total energy consumption. ICT equipment loads are iteratively estimated as in sub-chapter 4.1.2 to 1500 W (Mourão) and 1100 W (Montalegre). The results of both are represented in Figure 4-3 and Figure 4-4, respectively. The represented time periods for both locations are July, October and December; corresponding to a total of nine days.

Unlike the large containers, several load peaks occur in the measured energy consumption for both locations. From a visual perspective, the load peaks occur randomly with amplitude of 1500 W. These load peaks maybe appear due to a quick turning-on and off the additional AC split units. EnergyPlus only models the PTAC unit, thus the behavior of the AC Split units is not captured. Moreover, the resolution of the measurement for the small containers is small, because energy consumption is only measured one time step per hour. Thus, it is difficult to perform an accurate calibration.

Since the HVAC units are performing based on temperature sensor information, high internal temperatures may cause the switch-on of the additional AC split units. Thus, in a post-simulation check in Excel, the simulated total energy consumption is modified to achieve better fitting with the measured values. Here, the simulated values are correlated to the value of the interior temperature sensor T1 and modified subsequently. The modification of the simulated energy consumption for Mourão $E_{sim,modified,Mourao}$ is performed according to equation (4.2):

$$E_{sim,modified,Mourao} = \begin{cases} E_{sim} + 1500W, if\ [T1(t) > 24.5°C\ ] \\ E_{sim}, else \end{cases} \quad \textbf{(4.2)}$$

which describes that the obtained simulated energy is increased by 1500 W, if the container temperature at the same time step is above 24.5°C.

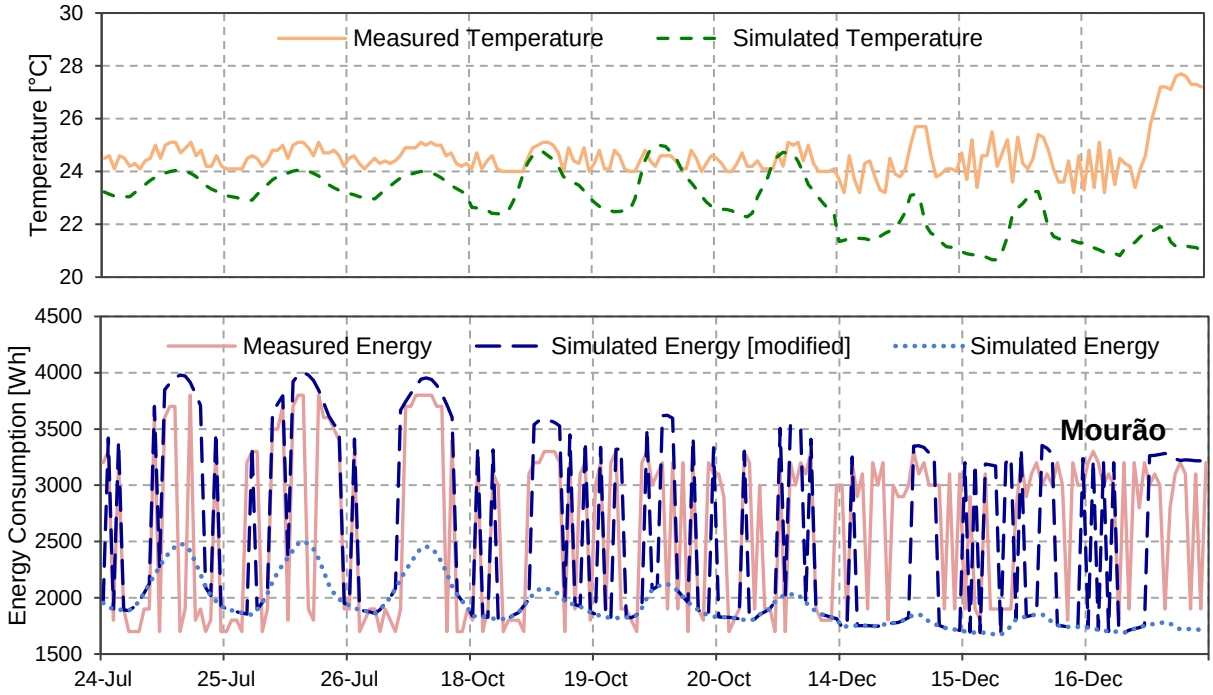

Figure 4-3: Manual calibration result for Mourão, measured and simulated temperature and energy consumption (with post-simulation modification)

The correction of the load consumption for Montalegre is depicted in the following equation:

$$E_{sim,modified,Montalegre} = \begin{cases} E_{simu} + 1500W, if\ [T1(t+1) < 23°C\ \wedge\ T1(t-(t+1)) > 1] \\ E_{sim}, else \end{cases} \quad (4.3)$$

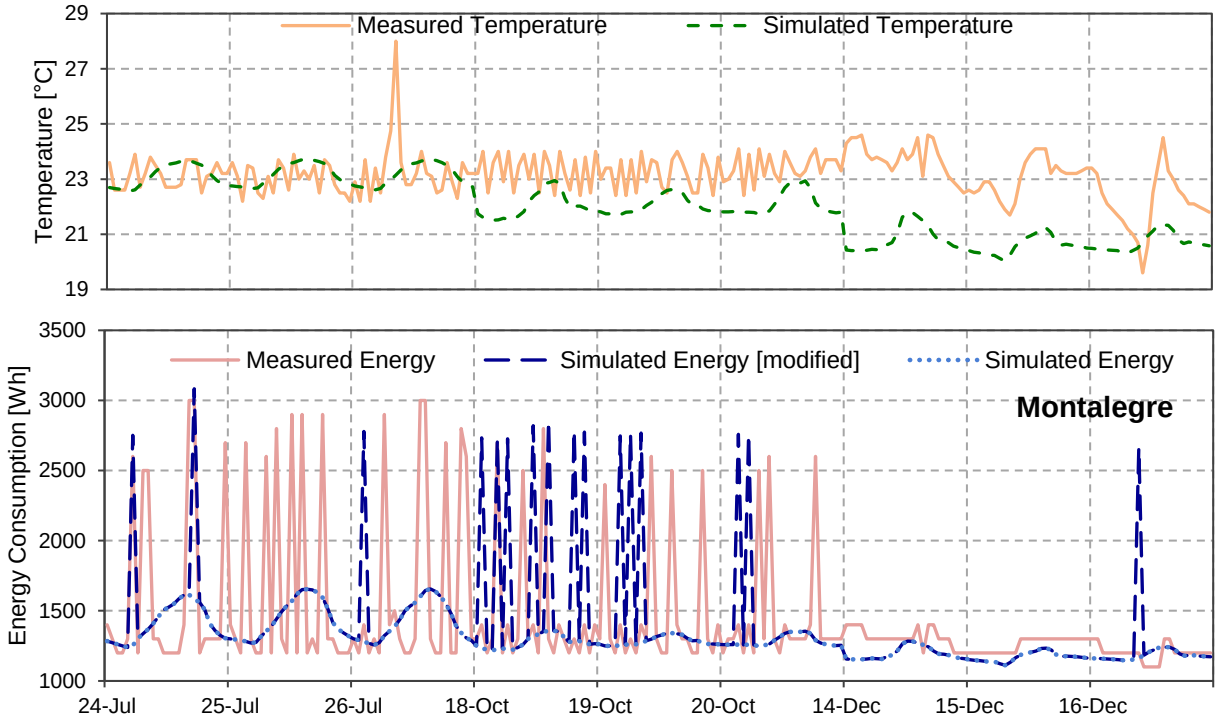

Figure 4-4: Manual calibration result for Montalegre, measured and simulated temperature and energy consumption (with post-simulation modification)

As visible in the previous plots, no equivalent results between modeled and measured data has been achieved for the small containers. Even in a modified simulation to capture the effects of the AC split units, no matching can be achieved. It should be related to unknown dynamics in these container, which are not being monitored by the existing sensors. Therefore, the calibration work is only possible for the two large containers.

4.2 Automated Model Calibration

This chapter describes the procedures to perform an automated model calibration. Two metrics to assess the performance of the automated calibration are introduced. The automated model calibration is performed using two different methods: parametric analysis and evolutionary algorithms (EAs). Initially, the theory behind the methods of parametric analysis and EAs are described. Then, the corresponding software to apply these methods, jEPlus and jEPlus+EA, are presented. Finally, the obtained results of both methods are presented.

4.2.1 Metrics for assessing performance

In this study, two metrics are used to assess the performance of the automated calibration. The consideration of both metrics allows preventing any calibration error due to errors compensation.
The first metric, Normalized Mean Bias Error (NMBE), is the average difference between measured and simulated data points. It is a good indicator of the overall behavior of the simulation model. Positive values mean that the model under-predicts measured data, and negative ones mean over-prediction. The error is estimated as (4.4):

$$NMBE\ (\%) = \frac{\sum_{i=1}^{n}(m_i - s_i)}{n \cdot \bar{m}} \cdot 100 \qquad \textbf{(4.4)}$$

where m_i and s_i are the respective measured and simulated data points for each model instance 'i'; n is the number of data points and $\bar{m}$ is the average of the measured data points. The main problem with the NMBE is that it is vulnerable to cancellation errors, where the sum of positive and negative values could reduce the value of NMBE. The index is normalized to be comparable with other metrics. Hence, a further measure of model error is also required.

The second metric, Coefficient of Variation of Root Mean Square Error (CV(RMSE)), measures the variability of the errors between measured and simulated values by assembling offset errors between measured and simulated data. It does not suffer from the cancellation effect. The error is calculated as (4.5):

$$CV(RMSE)\ (\%) = \frac{\sqrt{\left(\frac{\sum_{i=1}^{n}(m_i - s_i)^2}{(n-1)}\right)}}{\overline{m}} \cdot 100 \quad \textbf{(4.5)}$$

The reference values for hourly calibration methods are based on the ASHRAE Guideline 14 [57]. The report states a tolerance of 10% for NMBE and 30% for CV(RMSE). In this study, the container temperature error and energy consumption error between measurements and simulations are summarized to a sum error. It facilitates the result evaluation, as there are only two outputs, instead of four: sum of CV(RMSE) and sum of NMBE. Regarding the selection of the best solutions, both metrics should be as low as possible, but priority is given to the CV(RMSE), as it does not suffer from cancelation errors.

4.2.2 Parametric Analysis

The parametric analysis in this study is a method in which a series of simulations is run by software with systematically changes of value of parameters associated to one or more design variables. Modifying simultaneously several variables is the approach of the parametric simulations to explore distinctive design options. Parametric analysis methods are often reinforced with methods such as sensitivity analysis, to achieve more useful results. Parametric simulations allow finding the real optimum solutions if all the solutions in the design space are simulated. This method is typically not feasible due to the amount of required simulation time and computer resources. Thus, a parametric project can also be the basis for the development of optimization problems and predictive models, which are introduced in terms of evolutionary algorithms in sub-chapter 4.2.3.

4.2.3 Evolutionary Algorithms

Evolutionary algorithms are a class of optimization algorithms inspired by the Darwinian evolution theory, developed by Holland [58]. EAs are one of the most popular metaheuristic optimization methods, especially the sub-group Genetic Algorithms. They are convenient because they can handle continuous variables, discrete variables or both in the same optimization problem.

An optimization problem consists of finding the decision variables that minimize or maximize some objectives under certain constraints. A problem can have one or more objectives (single / multi-objective). Moreover, an optimization problem contains constraints that the decision variables have to satisfy. If for certain values of the decision variables the restrictions are satisfied, it is a feasible solution. Thus, the goal is to find the best solutions from all feasible solutions.

EAs have multiple benefits such as the fact that they are population based and are especially suitable for solving multi-objective problems. In multi-objective problems, the objective is to find Pareto optimal

solutions, which are the solutions of an optimization problem than cannot be improved in one objective without degrading at least one other objective. The Pareto Front consists of several Pareto optimal solutions that should be uniformly distributed along the front. They permit simultaneous evaluation of *n* individuals in a population, allowing parallel simulations on computers with multiple cores. They usually do not cause problems when simulation programs fail to evaluate specific solutions. In this study, EAs are applied in two cases: model calibration (sub-chapter 4.2.7) and multi-objective optimization model (sub-chapter 5.4).

The concept of EAs is the following: The process starts with implementing an encoding scheme for representing the solutions (the decision variables) in a numerical way that it can be handled by EAs. An encoding of a design solution is called a “chromosome”, in which each decision variable is encoded as a “gene”. Typically, the initial population of solutions is randomly sampled across the solution space. Each solution in the population will be evaluated for its “fitness” for a given set of criteria, using the objective function. As the optimization progresses, each population includes fitter and fitter solutions. The optimization process finally converges and is eventually dominated by a single solution. The ranking guarantees that the “fitter” solutions will have a higher chance to be used in making new variations. EAs use two operators to form novel solutions from existing ones: “crossover” and “mutation”. Crossover and mutation are nature-inspired ways for creating novel solutions (offsprings) from existing solutions (parents). In crossover two or more parents are combined to form offsprings. Mutation refers to random changes of the genes of the chromosomes. Encoding specific crossovers and mutation operators are often necessary for solving an optimization problem efficiently [59].

4.2.4 Software jEPlus

jEPlus [60] is a software package originally developed for creating parametric projects around EnergyPlus. Recently it has been expanded to work with other simulation programs. Parametric simulations are often used for investigating the effects of a selected few design options, or exploring the solution space of all design options as already described in sub-chapter 4.2.2.
jEPlus allows defining multiple parametric variables, each with their possible values, and then automatically create and run the required EnergyPlus simulation jobs. It permits users to extract and process the simulation results according to their requirements. One of the key benefits of jEPlus is that any part of the EnergyPlus model can be assumed as a parameter. The only requirement is that a search string (alternative block) can replace the single parameter. Each parameter definition contains several alternative values defined by the user. The design parameters are organized in a tree structure and stored with the EnergyPlus execution settings in a jEPlus project file. The program can simulate all possible combinations of the parameters in each project. In general, jEPlus allows managing and performing parametric studies, which would be difficult with manual simulation sets.

4.2.5 Software jEPlus+EA

jEPlus+EA is an extension software for jEPlus that allows performing optimization problems, coupling building simulation tools (EnergyPlus) and optimization algorithms, the so-called building design optimization.

The program applies the genetic algorithm optimization method NSGA-II (Nondominated Sorting Genetic Algorithm II) [61]. It has been adapted to use integer encoding and crossover-mutation operators. It is based on dominance ranking which ensures that non-dominated solutions are preferred over dominated ones. As many of the most advanced genetic algorithms, the NSGA-II has a multi-objective, population-based and elitist search method. This algorithm is recognized by its robustness and versatility.

Before starting the optimization process in jEPlus+EA, the user must define the decision variables (gens) and the optimization problem in a jEPlus project. The software encodes the different genes to a solution space (chromosomes). All necessary input files for running EnergyPlus simulations are referenced in the jEPlus project file, which includes the installation location of the EnergyPlus executable, weather file, simulation model files and the results extraction file (RVX). The RVX file contains the definition of the optimization problem and instructions for result extraction. Moreover, it contains additional features, such as a link to post-simulation processes wit Python[2], which is applied in chapter 4.2.6.

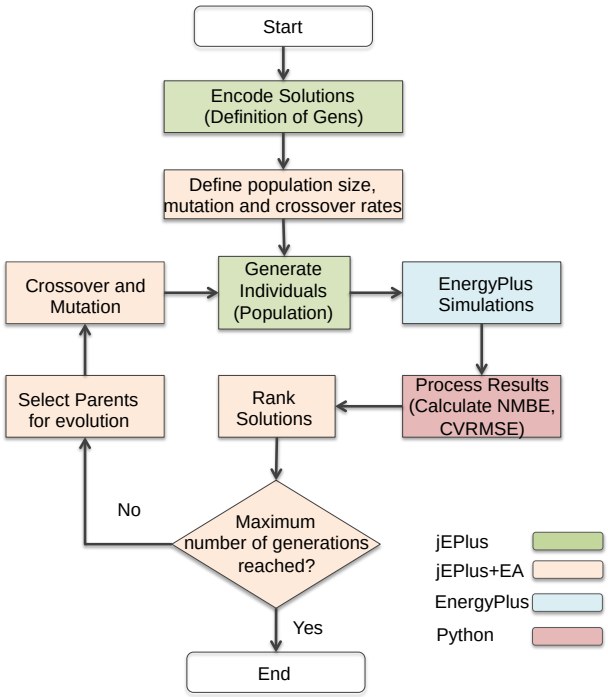

Figure 4-5: Flowchart of genetic algorithm procedure for calibration

[2] Python is a widely used programming language for general purpose programming

Once the jEPlus project is set, the jEPlus+EA tool can then be coupled with jEPlus. The flowchart of the genetic algorithm procedure for calibration is illustrated in Figure 4-5.

First the solutions are encoded, and an initial random population is produced. The user can define the initial population size. Then, the first generation is converted into a set of simulation jobs that is processed by EnergyPlus. The results are generated according to the RVX file definitions. In this case a Python script called, that calculates the calibration error metrics defined in 4.2.1.

Afterwards, the solutions are ranked by its fitness to reach the objectives (low error indices). The NSGA-II specified ranking method has two approaches that aim to create more distributed solution sets. Firstly, the solutions are sorted based on non-domination Pareto fronts. Less dominated Pareto fronts get better positions. Secondly, within the Pareto front, the crowding distance is calculated for each solution. The crowding distance is a measure of how close a solution is to its neighbors. Solutions that are more far from other solutions are better ranked [61].

In a next step the parents (two or more) of the next generation are selected. This process is called tournament and is based on the fitness and the crowding distance. The parents generate an offspring population with crossover and mutation operators.

As a result, the offspring solutions represent a new population that is simulated by EnergyPlus. Parents and offspring built a next generation that can be ranked again. The process is terminated manually by the user or when the predefined generation limit is reached. Nevertheless, the fact that these algorithms are designed to converge to optimal values, it is evident that not all solutions are assessed. Thus, it is probable that not all possible optimal solutions are found in the optimization procedure.

4.2.6 Calibration based on Parametric Analysis

The calibration variables are identified based on highest uncertainty and largest impact on the discrepancies between simulated and measured interior temperature and total energy consumption. An overview of the five calibration parameters and their value ranges is given in Table 4-3. The total size of the solution space is 2520.

Table 4-3: Calibration Parameters

Parameter	Value Range	Unit
Temperature Set point	20.0 / 20.5 / 21.0 / 21.5 / 22.0 / 22.5 / 23.0	°C
COP	3.4 / 3.5 / 3.63 / 3.7	-
ICT Equipment Power	5100 / 5200 / 5300	W
Infiltration Rate	0.1 / 0.2 / 0.4 / 0.5 / 0.6 / 0.7	ACH
Insulation Thickness	0.015 / 0.020 / 0.025 / 0.030 / 0.040	m

Simulated total energy consumption and operative temperature are compared to measured hourly total energy consumption and interior temperature (sensor T1). The analysis is performed using jEPlus (v1.7.0). In order to run 2520 solutions, simulations are executed remotely on the jEPlus Simulation Sever (JESS) [62]. A Python script is created and implemented in jEPlus to calculate both indices.

The simulation run period covers a three weeks period for both locations. To ensure more variety of outdoor conditions, the run period is split into three single weeks, where each week is of a different month. The selection of period is limited to the available measured raw data for each location. Cinfães simulation covers the months July, September and December of 2016; Salvaterra de Magos simulation includes January, February and March of 2017. The parametric analysis is only performed for Salvaterra de Magos, as the calibration with EAs produce equivalent results and is executed for both locations.

The 15 best solutions of the run are presented in Table 4-4, ordered ascending by the sum of CV(RMSE). For each solution, the parameter values and indices results are reported. The solution "G-0_2_0_4_2_1" is highlighted, because it has the best trade-off between the calibration metrics and it is also elected as the best solution in the calibration based on optimization in sub-chapter 4.2.7. This solution has an hourly sum of CV(RMSE) of 10.23% and sum of NMBE of 1.43%. Both values are within the ASHRAE standards of the previous sub-chapter 4.2.1. For all results, a COP value of 3.4 and an ICT equipment value of 5300 W are found, which validate two important assumptions that were done.

Table 4-4: Best 15 CV(RMSE) results of parametric analysis for Salvaterra de Magos

Solution Name	Insulation thickness [m]	COP [-]	Infiltration rate [ACH]	ICT equipment [W]	Temperature set point [°C]	Sum CV(RMSE) [%]	Sum NMBE [%]
G-0_1_0_5_2_2	0.020	3.4	0.7	5300	21.0	10.08	1.75
G-0_1_0_4_2_2	0.020	3.4	0.6	5300	21.0	10.09	1.73
G-0_3_0_3_2_2	0.020	3.4	0.5	5300	21.0	10.09	1.72
G-0_1_0_0_2_2	0.020	3.4	0.4	5300	21.0	10.10	1.71
G-0_1_0_1_2_2	0.020	3.4	0.2	5300	21.0	10.11	1.68
G-0_1_0_0_2_2	0.020	3.4	0.1	5300	21.0	10.12	1.67
G-0_0_0_5_2_2	0.015	3.4	0.7	5300	21.0	10.19	2.53
G-0_0_0_4_2_2	0.015	3.4	0.6	5300	21.0	10.19	2.51
G-0_0_0_3_2_2	0.015	3.4	0.5	5300	21.0	10.19	2.50
G-0_0_0_2_2_2	0.015	3.4	0.4	5300	21.0	10.19	2.49
G-0_0_0_1_2_2	0.015	3.4	0.2	5300	21.0	10.20	2.46
G-0_0_0_0_2_2	0.015	3.4	0.1	5300	21.0	10.20	2.44
G-0_2_0_5_2_1	0.025	3.4	0.7	5300	20.5	10.23	1.44
G-0_2_0_4_2_1	0.025	3.4	0.6	5300	20.5	10.23	1.43
G-0_2_0_3_2_1	0.025	3.4	0.5	5300	20.5	10.24	1.42

The results of all parametric solutions are plotted in Figure 4-6, showing a scatter plot to illustrate the spread of the solutions for Salvaterra de Magos. Values are between 1% and 18% for sum of NMBE and between 10% and 21% for sum of CV(RMSE). The chosen solution "G-0_2_0_4_2_1" is again highlighted as a red dot.

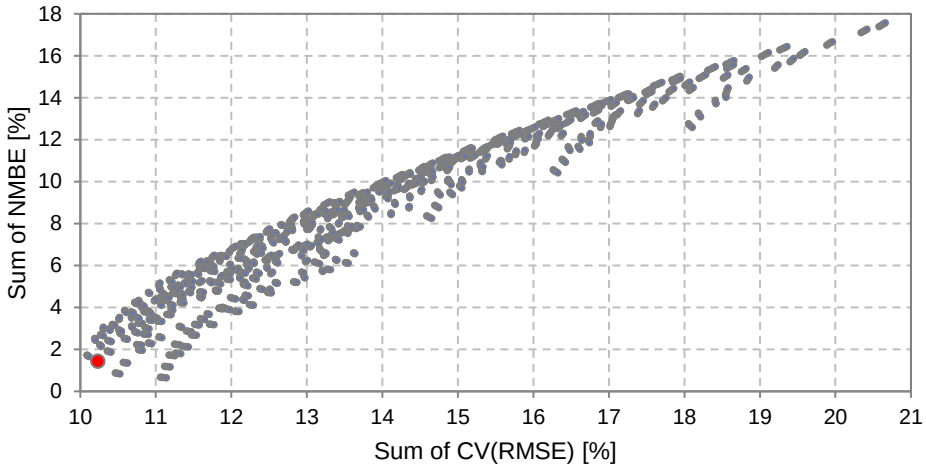

Figure 4-6: Scatter plot of 2520 solutions of parametric analysis for Salvaterra de Magos

The parametric analysis can identify the solutions with the best trade-off for both error metrics and can give a total picture of all possibilities. However, the method is very time consuming and resource demanding, especially for complex building simulations. Thus, in a next step, calibration is performed based on optimization to decrease simulation time and resources.

4.2.7 Calibration based on Evolutionary Algorithms

This sub-chapter describes an automated model calibration based on optimization. This method can obtain equivalent results and is less time consuming, compared to the parametric analysis in the previous chapter 4.2.6. Building energy model calibration is a quite new application of optimization.
The software jEPlus+EA (v1.7.6) is used to implement the EA-based (NSGA-II algorithm) calibration approach. In the study case, two objective functions are set for minimization: the sum of CV(RMSE) and the sum of NMBE. The problem is formulated according to (4.6):

$$\mathrm{Min}\{SumCVRMSE(\vec{x}), SumNMBE(\vec{x})\}, \vec{x} = [x_1, x_2 \dots x_m] \quad \textbf{(4.6)}$$

With:

$\vec{x}$ = Vector of the decision variables

m = Number of decision variables

A Python script estimates both errors and gives the result back to the evolutionary algorithm. The algorithm uses the default settings of jEPlus. The population size of the evolutionary algorithm is set to

10 individuals, while the number of generations is limited to 30. The value of 30 generations is identified after a few tests with different generations numbers, as it gives satisfying results and computational time is reduced. The crossover rate, that is the creation of novel solutions based on existing ones, is set to the maximum of 1. The mutation rate (random changes to novel solutions) is fixed to 0.2. The value is low to prevent a trial and error optimization method. The simulation run period is like the parametric calibration in sub-chapter 4.2.6.

Figure 4-7 demonstrates the results of both optimization runs after 30 generations. Compared to the parametric analysis, less than 10% of the computational time is needed. The results for Salvaterra de Magos are shown on the left, and on the right, the ones for Cinfães. The Pareto optimal solutions are marked as red dots. The blue dots are the solutions of the current generation (in this case generation 30). Both runs show an identical shape of the scatter plot. The best solutions for Salvaterra de Magos start at 10% for sum of CV(RMSE) and at 0.8% for sum of NMBE, while for Cinfães at 7% and 0.2%.

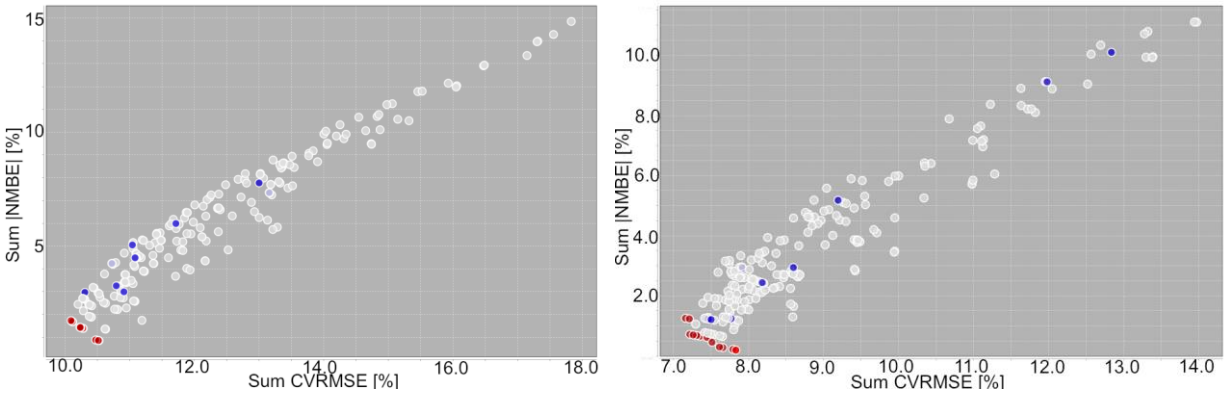

Figure 4-7: Scatter plots results of calibration based on optimization after 30 generations for Salvaterra de Magos (left) and Cinfães (right), with sum of CV(RMSE) on the x-axis, against sum of NMBE on the y-axis. Red dots are Pareto optimal solutions, while blue dots are solutions of the last generation.

A detailed insight of the Pareto optimal solutions for Salvaterra de Magos is given in Table 4-5. Equal to the parametric analysis, the optimization run can identify the highlighted solution “G-0_2_0_4_2_1”, which has the best trade-off of both indices. The parameter options of the calibrated solution are all different to the initial parameter settings in the manual calibration. In total 14 Pareto optimal solutions are found.

Table 4-5: Pareto optimal solutions of calibration based on optimization after generation 30 for Salvaterra de Magos

Solution Name	Insulation thickness [m]	COP [-]	Infiltration rate [ACH]	ICT equipment [W]	Temperature set point [°C]	Sum of CV(RMSE) [%]	Sum of NMBE [%]
G-0_3_0_0_2_1	0.030	3.4	0.1	5300	20.5	10.52	0.85
G-0_1_0_4_2_2	0.020	3.4	0.6	5300	21.0	10.09	1.73
G-0_3_0_4_2_1	0.030	3.4	0.6	5300	20.5	10.47	0.88
G-0_2_0_0_2_1	0.025	3.4	0.1	5300	20.5	10.28	1.39
G-0_2_0_5_2_1	0.025	3.4	0.7	5300	20.5	10.23	1.44
G-0_1_0_0_2_2	0.020	3.4	0.1	5300	21.0	10.12	1.67
G-0_3_0_3_2_1	0.030	3.4	0.5	5300	20.5	10.48	0.88
G-0_3_0_1_2_1	0.030	3.4	0.2	5300	20.5	10.51	0.86
G-0_2_0_1_2_1	0.025	3.4	0.2	5300	20.5	10.27	1.39
G-0_2_0_3_2_1	0.025	3.4	0.5	5300	20.5	10.24	1.42
G-0_1_0_1_2_2	0.020	3.4	0.2	5300	21.0	10.11	1.68
G-0_1_0_2_2_2	0.020	3.4	0.4	5300	21.0	10.10	1.71
G-0_2_0_4_2_1	0.025	3.4	0.6	5300	20.5	10.23	1.43
G-0_1_0_3_2_2	0.020	3.4	0.5	5300	21.0	10.09	1.72

In Table 4-6 are shown the Pareto optimal solutions for Cinfães. In total, 13 solutions are found after 30 generations. The solution with the best trade-off is “G-0_3_0_5_1_4”, which has a sum of CV(RMSE) of 7.22% and a sum of NMBE of 0.72%. This calibrated solution is different in all parameters, compared to the initial parameter settings in the manual calibration of Cinfães.

Table 4-6: Pareto optimal solutions of calibration based on optimization after generation 30 for Cinfães

Solution Name	Insulation thickness [m]	COP [-]	Infiltration rate [ACH]	ICT equipment [W]	Temperature set point [°C]	Sum of CV(RMSE) [%]	Sum of NMBE [%]
G-0_4_0_5_1_4	0.040	3.4	0.7	5200	22	7.16	1.25
G-0_2_3_0_2_4	0.025	3.7	0.1	5300	22	7.83	0.19
G-0_3_0_5_1_4	0.030	3.4	0.7	5200	22	7.22	0.72
G-0_3_3_3_2_4	0.030	3.7	0.5	5300	22	7.51	0.46
G-0_2_3_4_2_4	0.025	3.7	0.6	5300	22	7.61	0.30
G-0_2_3_3_2_4	0.025	3.7	0.5	5300	22	7.66	0.28
G-0_3_0_2_1_4	0.030	3.4	0.4	5200	22	7.35	0.66
G-0_3_0_1_1_4	0.030	3.4	0.2	5200	22	7.45	0.62
G-0_3_0_0_1_4	0.030	3.4	0.1	5200	22	7.49	0.59
G-0_3_0_3_1_4	0.030	3.4	0.5	5200	22	7.31	0.68
G-0_3_0_4_1_4	0.030	3.4	0.6	5200	22	7.26	0.70
G-0_2_3_1_2_4	0.025	3.7	0.2	5300	22	7.79	0.22
G-0_4_0_4_1_4	0.040	3.4	0.6	5200	22	7.21	1.23

Figure 4-8 illustrates the calibrated solution for Salvaterra de Magos graphically. The container temperature and the energy consumption are plotted over the three weeks simulation period. It is visible that the simulated outputs are mostly matching the measurements. The simulation shows only peak per day, although various small peaks per day occur sometimes in the measurements. This discrepancy can be related to the uncertainty of the energy meter itself.

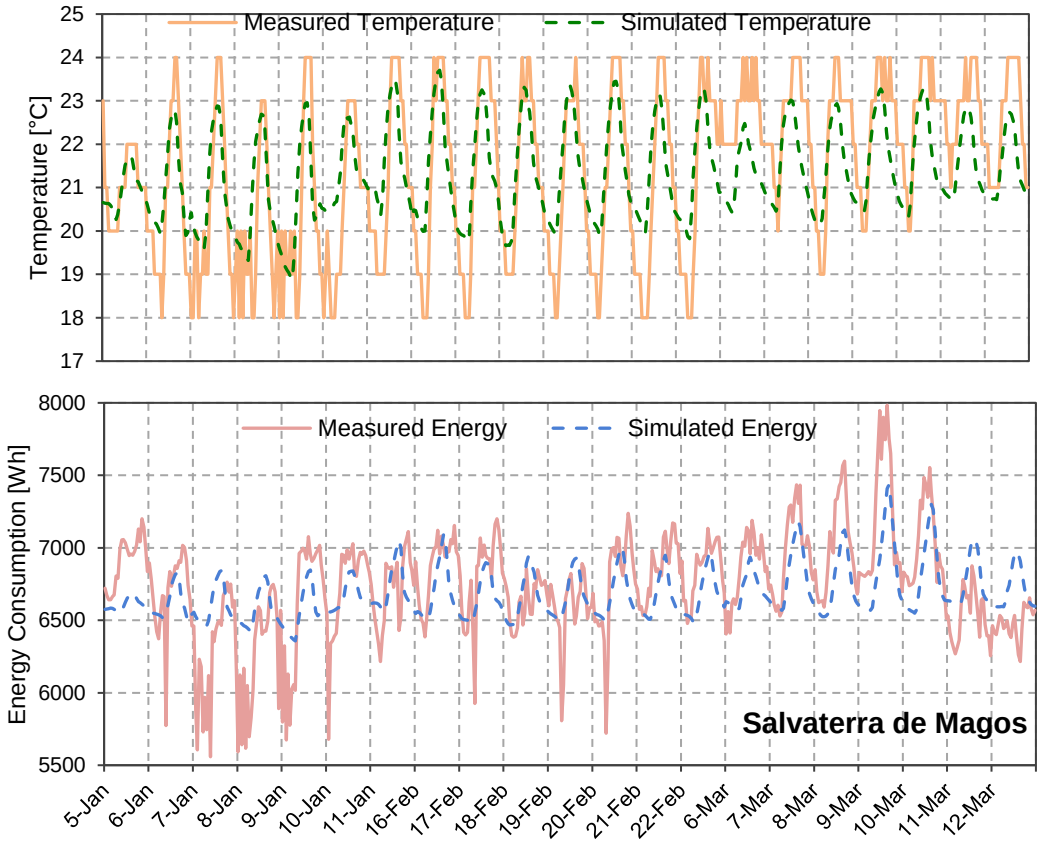

Figure 4-8: Calibrated model solution "G-0_2_0_4_2_1" for Salvaterra de Magos: comparison of measurement and simulation of temperature and energy consumption

Figure 4-9 represents the calibrated solution for Cinfães and gives a quick visual insight of the matching of simulation and measurement. The simulation reproduces the measured energy consumption quite well. The difference of summer and winter is observable: in summer, the consumption differs much more between day and night due to the high daily outside temperatures. The simulated container temperature displays some over prediction in September of about 1°C and some discrepancies in December, however it provides a good fit in July. These discrepancies may be explained by the fact that the exact location of the temperature sensor is unknown and measured temperature may correspond to a point in the container that does not sense representative container temperatures.

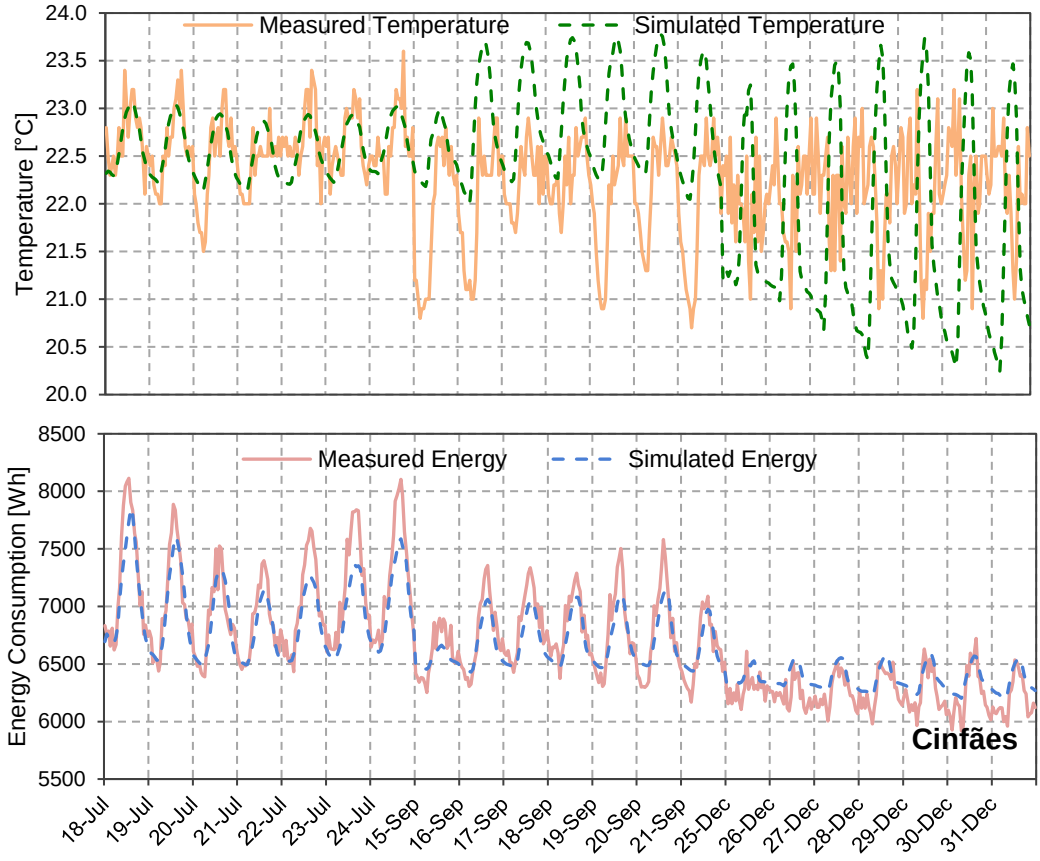

Figure 4-9: Calibration model solution "G-0_3_0_5_1_4" for Cinfães: comparison of measurement and simulation of temperature and energy consumption

Resulting from the simulations, the energy needed to run the HVAC is about 16% (December) up to 33% (July) of the total energy consumption for Cinfães. For Salvaterra de Magos, HVAC energy is estimated as 17% (January) up to 28% (March) for the simulated time period.

4.3 Sensitivity Analysis

This chapter offers a detailed description of the sensitivity analysis of the automated calibration results. To observe the relative impact of each design variable, the Morris and Sobol sensitivity methods are applied. The results of both methods are presented and compared.

4.3.1 Introduction

Sensitivity analysis can give an understanding about the impact of the inputs on the outputs in a system. The analysis is based on the automated calibration with jEPlus+EA in the previous sub-chapter 4.2.7. The calibration results of the two large containers Cinfães and Salvaterra de Magos are analyzed. During this analysis, the effect of five input factors on four outputs factors are evaluated. The input factors are the five decision variables temperature set point, ICT equipment power, insulation thickness, COP and infiltration rate. The output factors are sum of CV(RMSE) and sum of

NMBE of container temperature and total energy consumption. Morris and Sobol methods for sensitivity analysis are applied to investigate the impact of each variable. Both methods are global sensitivity methods, which means that the variation of outputs is evaluated, due to the simultaneous variation of the inputs. Sensitivity analysis can help to identify the relative impact of the design variables on the calibration error and consequently on the indoor temperature level and energy performance of the containers [63].

The sensitivity analysis is performed using jEPlus, EnergyPlus and the software SimLab, which is a free tool designed for sensitivity and uncertainty analysis. A flowchart of the entire process is represented in Figure 4-10. The jEPlus projects of Cinfães and Salvaterra de Magos that are developed in chapter 4.2.7 provide the information (design variables and simulation model) for the sub-sequent simulations. The first step in SimLab is the definition of the input factors, which are the design variables of the calibration projects. It implicates the definition of the weights and the probability distribution of the input factors. All input factors are described by discrete uniform distributions and their values are weighted equally.

Table 4-7: General definition of input factors for sensitivity analysis

Input Factor/Parameter	Units	Steps	Increment	Minimum	Maximum
Temp. Set Point	°C	7	0.5	20.0	23.0
ICT Equipment Power	W	3	100	5100	5300
Insulation Thickness	m	5	uneven	0.015	0.040
COP	-	4	uneven	3.4	3.7
Infiltration Rate	ACH	6	uneven	0.1	0.7

In the next step the statistical pre-processor module of SimLab creates the Morris and Sobol sample matrix, where a sample of solutions for different combinations of input factors of Table 4-7 is generated. The sample size depends on the method of sensitivity analysis. Subsequently, the samples are simulated in EnergyPlus through the interface of jEPlus. With the EnergyPlus simulation results, a customized output text file (output model) is created, that SimLab can read. Then the output model and the solutions sample are executed in SimLab, where the statistical post-processor module of the program performs the sensitivity analysis. Finally, the results of the sensitivity analysis are extracted from SimLab and processed further in Excel for comparison.

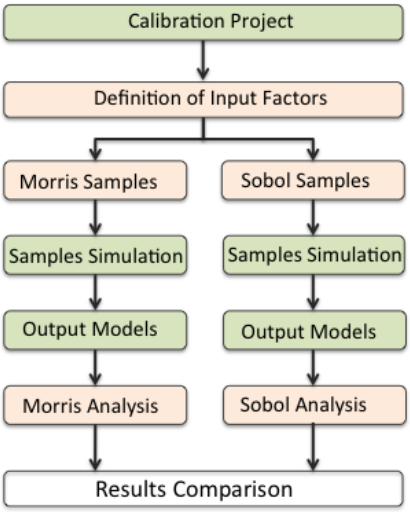

Figure 4-10: Flowchart of Sensitivity Analysis of Calibration in jEPlus/EnergyPlus (green) and SimLab (orange)

4.3.2 Morris Method

The Morris method is a global sensitivity analysis [64]. It consists of two sensitivity indexes, Mu (μ) and Sigma (σ). The Mu index shows the impact of the input factor on the outputs. A higher value represents a greater impact. The Sigma index presents an overall measure of the interactions with other factors and the nonlinear effects [65]. A higher value means greater non-linear effects of the variable. This method generates randomized ”one-factor-at-a-time” experiments to see the effect of changing a value of one input factor. The number of model simulations required for the Morris method is estimated as $r\ (k+1)$. In this equation, k represents the number of input factors (design variables), which are 5 in this study. The trajectories r are 10 in this case, which is the maximum value allowed. Trajectories are sequences of step-wise parameter changes. Thus, considering that there are 10 trajectories, each trajectory with 5+1 sampling points, 60 model simulations are generated in a sample [65].

4.3.3 Sobol Method

The Sobol method has the objective to estimate the impact of each decision variable to the whole model output and its interaction with the other decision variables [66]. It is a variance-based method, which means the variance of the output due to every input variable is quantified. This method uses two principal sensitivity indices: the first order effect and total effect. The first order effects represent the output variations linked to the corresponding inputs. The total effects estimate the total contributions to the corresponding input to the output variance. It includes first order and higher order effects. The difference of first order effects and total effects show the impact of interactions between input variables.

The sample size of the Sobol methods depends on the number of decision variables and the model complexity. First order and total order index corresponds to a sample size of $n\ (2k + 2)$, where k is the number of variables and n as the number of model executions for calculating one individual effect. To obtain a more accurate and stable result the largest possible value n =128 is chosen. Thus, a sample size of 1536 samples is generated.

4.3.4 Morris sensitivity analysis results

The results of the sensitivity analysis using Morris method for both Cinfães and Salvaterra de Magos are shown in a group of plots in Figure 4-11. In the results, the five design variables of the model calibration are considered: *interior temperature set point, insulation thickness, ICT equipment power, COP* and *infiltration rate*. The four output factors are the sum of CVRMSE and sum of NMBE of operative container temperature and total energy consumption. Each individual plot shows indexes Mu (μ) and Sigma (σ) for one output factor. The Mu index shows the importance of each variable on the output, while the Sigma index describes the interaction (non-linear effects) between each input. Large values represent a strong importance, therefore a strong interaction. Both indices are normalized, such that the maximum value is always 1.

The figures show that *interior temperature set point* has a strong impact in both locations for the operative temperature as input and output are directly linked. On the other hand, energy consumption has a medium to low influence. *Insulation thickness* shows a medium influence for the operative temperature in Cinfães, while for Salvaterra de Magos the impact is medium to high. Moreover, the influence on other input variables is strong for the operative temperature for both locations. In terms of energy consumption, the relative impact of *insulation thickness* is medium to low.

ICT equipment power has nearly zero impact on the operative temperature for both locations. This makes sense, because the variation of this parameter is small, and the HVAC system is always able to remove the generated heat loads, also the maximum value of 5300 W. Regarding the energy consumption, the *ICT equipment power* has the most importance and greatest influence on other input variables as input and output factor are directly related. *COP* shows an impact on the operative temperature for both locations. Energy consumption value is medium influenced by the *COP* value; only for Cinfães the *COP* has a medium interaction with other input variables. Finally, *Infiltration rate* has zero impact on the energy consumption and operative temperature output value for both locations.

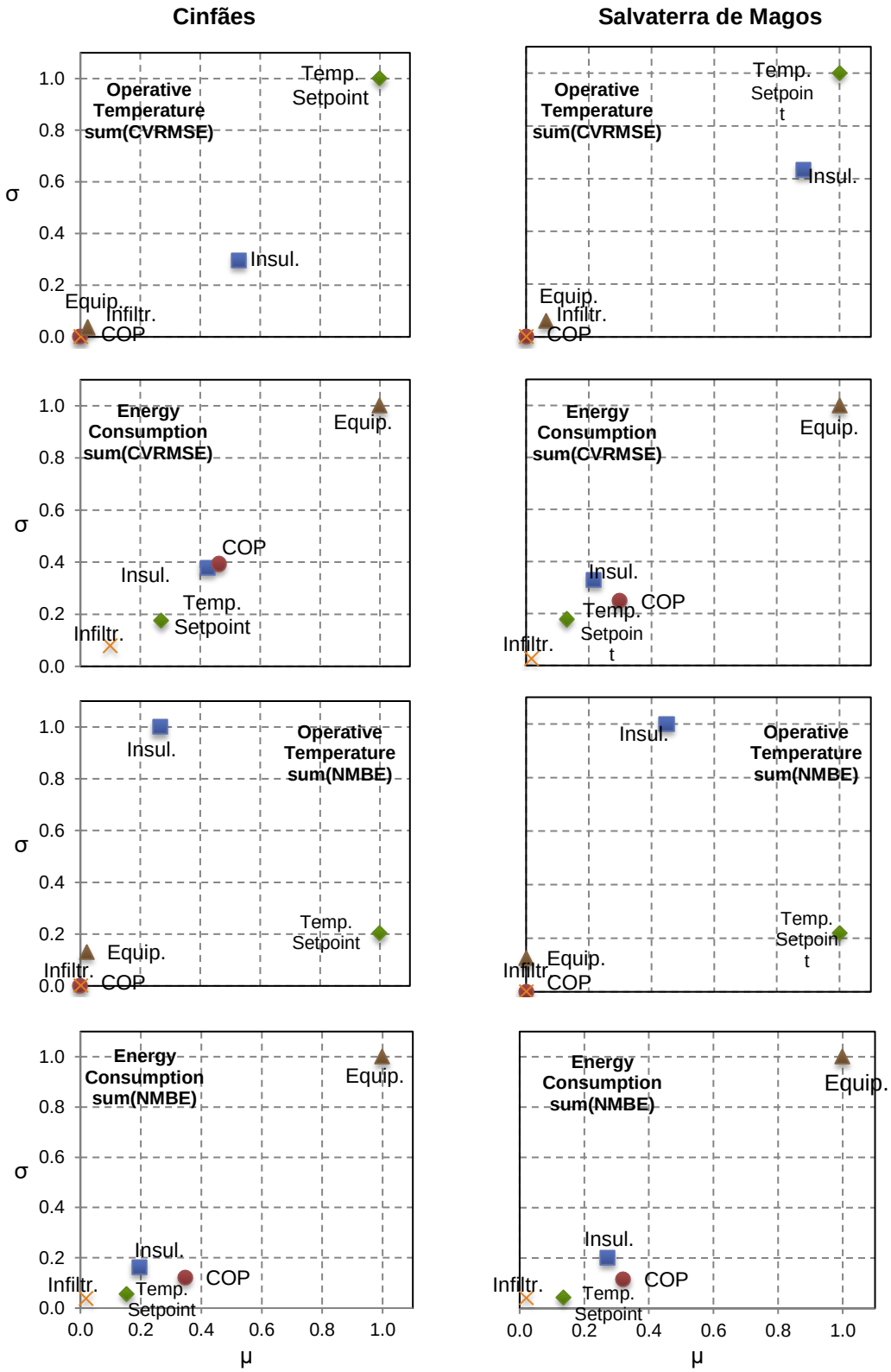

Figure 4-11: Results of Morris Method for Cinfães (left) and Salvaterra de Magos (right)

4.3.5 Sobol sensitivity analysis results

The group of plots that is printed in Figure 4-12 shows the results of the Sobol method for Cinfães and Salvaterra de Magos. Each plot represents the impact of the five design variables on one output

factor. The impact of each variable is described with the first order indices (red) that should sum 1, if the problem is fully linear. In this study, the totals are less than 1, because the problem is nonlinear. Moreover, the differences of the total effect indices and the first order indices (light red) are shown. The differences indicate the interactions with other design variables.

Interior temperature set point has strong influence on the operative temperature for both CVRMSE and NMBE in Cinfães and Salvaterra de Magos. Regarding the energy consumption, it has an incipient impact. *ICT equipment power* shows only impact to the energy consumption for both locations. The impact is strong, as *ICT equipment power* and energy consumption are directly related. *Infiltration rate* has zero influence in all plots as it is analyzed with the Morris method. *COP* shows some marginal influence on energy consumptions. *Insulation thickness* has a medium to low influence on the operative temperature for both locations. Moreover, it has low impact on the energy consumption.

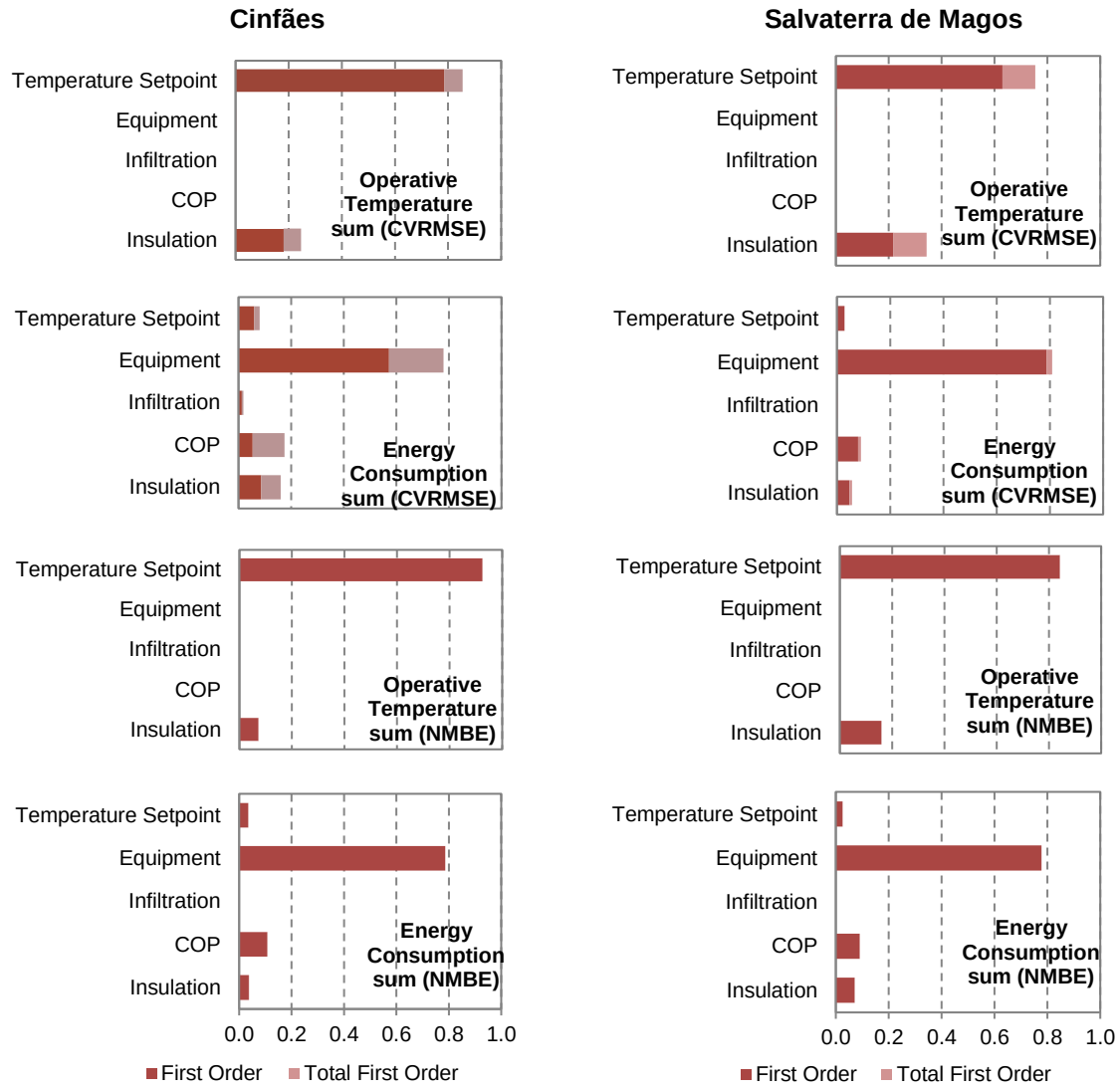

Figure 4-12: Results for Sobol First Order Index and as well the difference between them and Total Order Effects for Cinfães (left) and Salvaterra de Margos (right)

4.3.6 Comparison of both sensitivity methods

The results of the sensitivity analyses in this research identify the level of influence of each design variable on the calibrated output factors operative temperature and energy consumption. Both methods can identify the general sensitivity trend, although there are some minor differences.

In terms of operative temperature, both methods detect *temperature set point* followed by *insulation thickness* as the most influential input factors for both locations. Also, both agree that *infiltration rate*, *COP* and *ICT equipment power* have no impact on operative temperature. A more detailed comparison between both locations indicates that *insulation thickness* has predominantly more impact in Salvaterra de Magos. That difference to Cinfães may be explained with a generally warmer climate in Salvaterra de Magos.

Regarding energy consumption, Morris and Sobol method conclude that *ICT equipment power* has the notoriously the most impact. In addition, both methods indicate minor influences of *COP*, *temperature set point* and *insulation thickness* on the energy consumption. Finally, *infiltration rate* does not play a role in both methods. Although *infiltration rate* is identified as unimportant in this sensitivity analysis, it can still gain importance in some conditions, such as very cold climatic outdoor conditions.

Both sensitivity methods give qualitative data about the relative importance of the input factors. The Morris method gives the advantage of having low computational cost. As the Sobol methods is very detailed, but needs a lot of simulation time, it is less beneficial for complex simulation models.

5 Multi-Objective Optimization

In this chapter, the calibrated thermal simulation models are optimized regarding their energy consumption and associated cost. A multi-objective optimization (MOO) method is applied, which is introduced briefly in the first section. Following up, a time-sensitive tariff for different tariff options in the optimization model is introduced, which influences the optimization when considering cost. Subsequently, the individual solution for optimizing the containers are introduced and their energetic performance is presented. Ultimately the individual solutions are combined in whole MOO models to identify the best combinations of solutions.

5.1 Introduction

MOO is a mathematical optimization problem with more than one objective and can be especially helpful in dealing with conflicting criteria and trade-off relationships. It is broadly used where building simulation software is coupled to an optimization engine. MOO problems do not require a single optimum solution, but rather a set of single solutions with different objective functions, which are the so-called Pareto optimal solutions, as explained before in this thesis. These solutions can give an understanding about trade-off relationships between the single objectives. Evolutionary Algorithms (EAs) are powerful problem solvers, especially when dealing with multi-objective optimization problems. The nature of EAs and optimization problems were introduced in the previous sub-chapter 4.2.3. In this study, the objectives are the minimization of energy costs and investment costs. For solving the MOO problem, it is used the software jEPlus+EA, which is coupled with EnergyPlus for executing the simulations. The simulations are executed remotely with JESS to accelerate the simulation process.

5.2 Time-Sensitive Tariff

In order to be able to execute the simulations for single solutions in sub-chapter 5.3 and optimization model in sub-chapter 5.4, it is introduced a time-sensitive tariff of EDP (Energias De Portugal) that allows to display energy costs in the results [67]. An overview of the hourly prices per kWh and the time schedules is shown in Table 5-1, which are the same for any day of the week (daily cycle) The weekly cycle, which distinguishes week days from Saturdays and Sundays is not considered in this thesis. The summer schedule starts at 25th March and the winder schedule starts at 28th October. The contracted power for both locations is 20.7 kVA.

Table 5-1: Overview of time-sensitive tariff [67]

Tariff Type	Daily Period	Price [EUR/kWh]	Summer [Hours]	Winter [Hours]
Simple	Standard	0.1659	Always	Always
Dual-rate	Peak hours	0.1981	08:00 – 22:00	08:00 – 22:00
	Off-peak hours	0.1023	22:00 – 08:00	22:00 – 08:00
Tri-rate	Peak hours	0.2247	10:30 – 13:00 19:30 – 21:00	09:00 – 10:30 18:00 – 20:30
	Shoulder hours	0.1768	08:00 – 10:30 13:00 – 19:30 21:00 – 22:00	08:00 – 09:00 10:30 – 18:00 20:30 – 22:00
	Off-peak hours	0.1023	22:00 – 08:00	22:00 – 08:00
Contracted Power 20.7 kVA: 26.90 EUR/month				

5.3 Individual Solutions for Optimization

This section introduces seven individual solutions with the objective to optimize the containers energy performances. The single solutions are included in the EnergyPlus models of the calibrated solutions of sub-chapter 4.2.7. The simulations are executed sub-sequently in EnergyPlus. As it was done for the calibration, the runtime period comprises of three weeks with each week of a different month. Investment costs are not considered for the individual solutions.

5.3.1 Roof Shading

This individual solution consists of a simple opaque shading device mounted on the roof of the containers. As shading devices typically can reduce internal temperatures of buildings in warm climates, this solution is examined for application in MDCs. The model is drawn in SketchUp and is illustrated in Figure 5-1. As shown in the figure, it can provide significant shading to the roof; only in the early mornings and late afternoons a fraction of maximum 30% may be unshaded. The area of the shading device is equal to the roof area (14.78 m^2) and has a gap of 0.1 m to the roof.

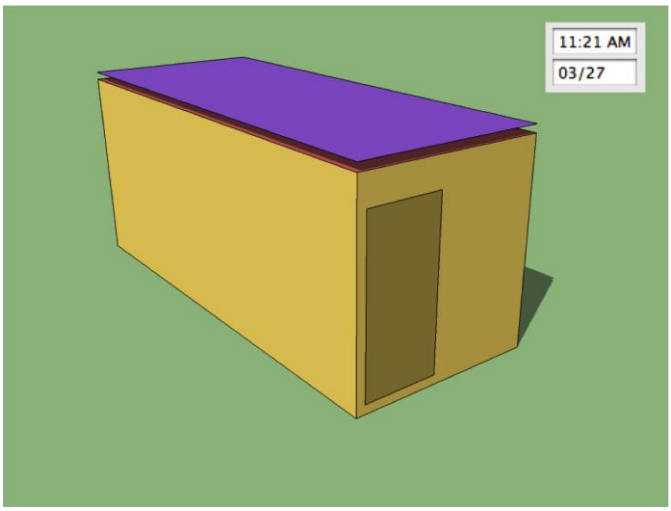

Figure 5-1: SketchUp container model with roof shading device

The simulation results for the shading device on the roof are presented in Figure 5-2 for both locations. It may be observed that no significant total savings in facility energy consumption are achieved, compared with the calibrated solutions. Salvaterra de Magos has reductions of 0.09%, while Cinfães can save slightly more: 0.31%, which corresponds to the warmer time periods of July and September.

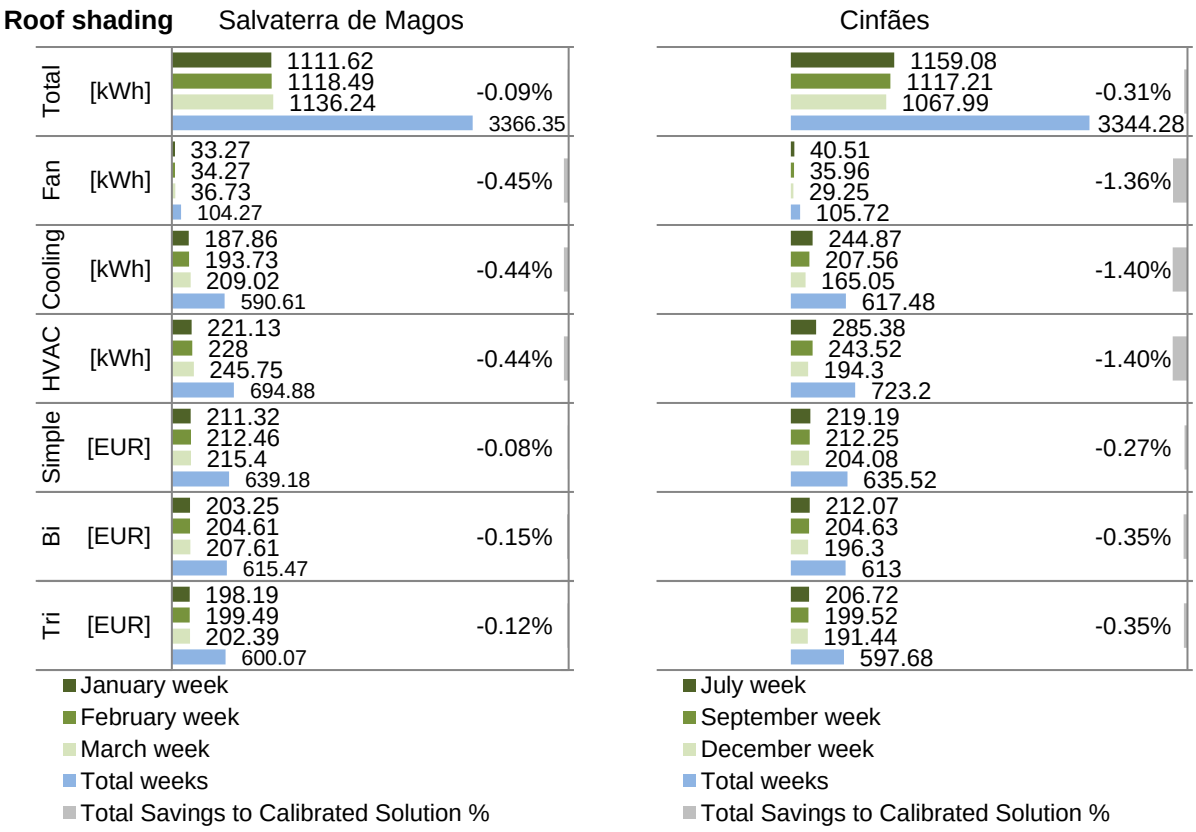

Figure 5-2: Optimization results for individual solution for Salvaterra de Magos (left) and Cinfães (right): Roof shading device. Overview of energy consumption (total facility/fan/cooling/HVAC) and energy costs (simple tariff/dual-rate tariff/tri-rate tariff) for week and total weeks time period. Each output includes actual savings [%] to calibrated solution for total weeks time period.

Regarding the energy costs, the tri-rate tariff is favorable for both sites, with costs of 600 EUR for Salvaterra de Magos and 598 EUR for Cinfães, which corresponds to cost reductions of 0.12% and 0.35%, respectively, compared to calibrated solutions.

5.3.2 Photovoltaic Panels

The following passage introduces a solution using renewable energies, where the shading device is equipped with nine photovoltaic panels. Due to the intense solar radiation and large numbers of sun hours in Portugal, this solution could be attractive for MDCs. This is the maximum number of panels fitting on the surface area without inclination. The specifications of the panels “SolarWorld SW 175” are presented in Table 5-2. The panel type is especially deployable for remote applications. Its module efficiency is 13.42%, with a maximum power of 175 Wp. In EnergyPlus, the PV panels are included within the module “PhotovoltaicPerformance:Sandia”, which consists of a series of empirical relationships with coefficients that are resulting from actual testing. The Sandia module allows to integrate PV panel specifications from the SAM library “2015.6.30”, developed by Sandia National Lab [68]. An inverter module is added to the EnergyPlus module, to convert the DC output to AC. The efficiency is assumed to be 90% and the radiative fraction is supposed to be 25%. As the inverter is inside the container, additional heat gains may be accounted by the simulation.

Table 5-2: Specifications of photovoltaic panels "SolarWorld SW 175" [69]

SolarWorld SW 175		
Parameter	Value	Unit
Maximum power	175	Wp
Open circuit voltage	44.4	V
Maximum power point voltage	35.8	V
Short circuit current	5.30	A
Maximum power point current	4.89	A
Module efficiency	13.42	%
Area	810 x 1610	mm
Cell Type	monocrystalline silicon	

The container drawing with the PV panels is shown in Figure 5-3. The panels do not shade each other, as they are mounted horizontally.

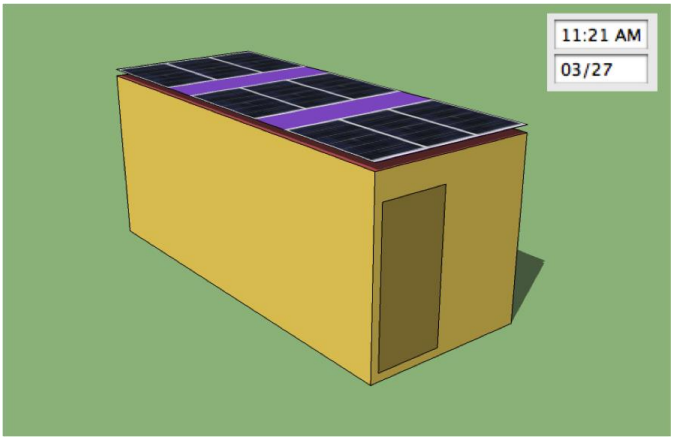

Figure 5-3: SketchUp container model with nine photovoltaic panels mounted on top of the roof

The optimization results with photovoltaic are included in Figure 5-4. In a run period of three weeks, the PV panels can save 3.02% of facility energy consumption for Salvaterra de Magos. In Cinfães, the energy is reduced by 4.21%. Cinfães has some more savings in HVAC energy due to the warmer simulated period for this container, where shading has a higher effect on HVAC consumption.

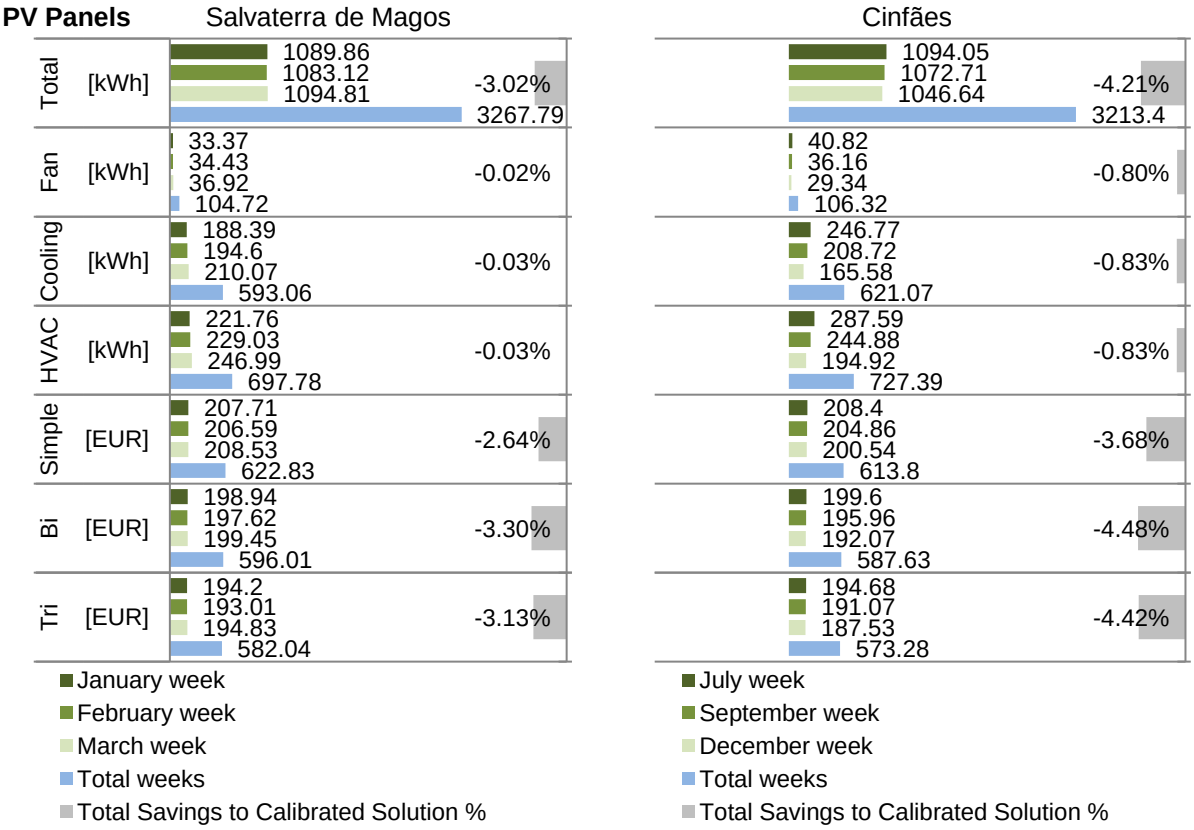

Figure 5-4: Optimization results for individual solution for Salvaterra de Magos (left) and Cinfaes (right): 9 PV Panels (and roof shading). Overview of energy consumption (total facility/fan/cooling/HVAC) and energy costs (simple tariff/dual-ratel tariff/tri-rate tariff) for week and total weeks time period. Each output includes actual savings [%] to calibrated solution for total weeks time period.

Reductions in terms of costs are equal to the energy consumption savings in both. The tri-rate tariff may be the cheapest, which leads to a total of energy costs of 582 EUR and 573 EUR, respectively.

5.3.3 Tree Shading

This solution picks up the idea of natural green shading. As tree shading has the potential to reduce indoor temperatures and to create energy savings in residential buildings in warm climates [70], this solution is applied on MDCs. A quantity of three trees are “planted” next to the containers. The tree species are pine trees, which are typical in warm southern European climate zones. Tree height is about 5.70 m with a simplified tree crown diameter of 4.70 m. The trees are arranged east, south and west from the containers. The corresponding SketchUp model is presented in Figure 5-5 with surface shadings in March.

Figure 5-5: SketchUp container model shaded by three pine trees (march morning)

Figure 5-6 presents the simulation results for both containers. The effects of tree shading are small and mostly identical: total energy consumption in Salvaterra de Magos is decreased by 0.20% and in Cinfães by 0.22%. HVAC energy is about 1.0% less in both cases.

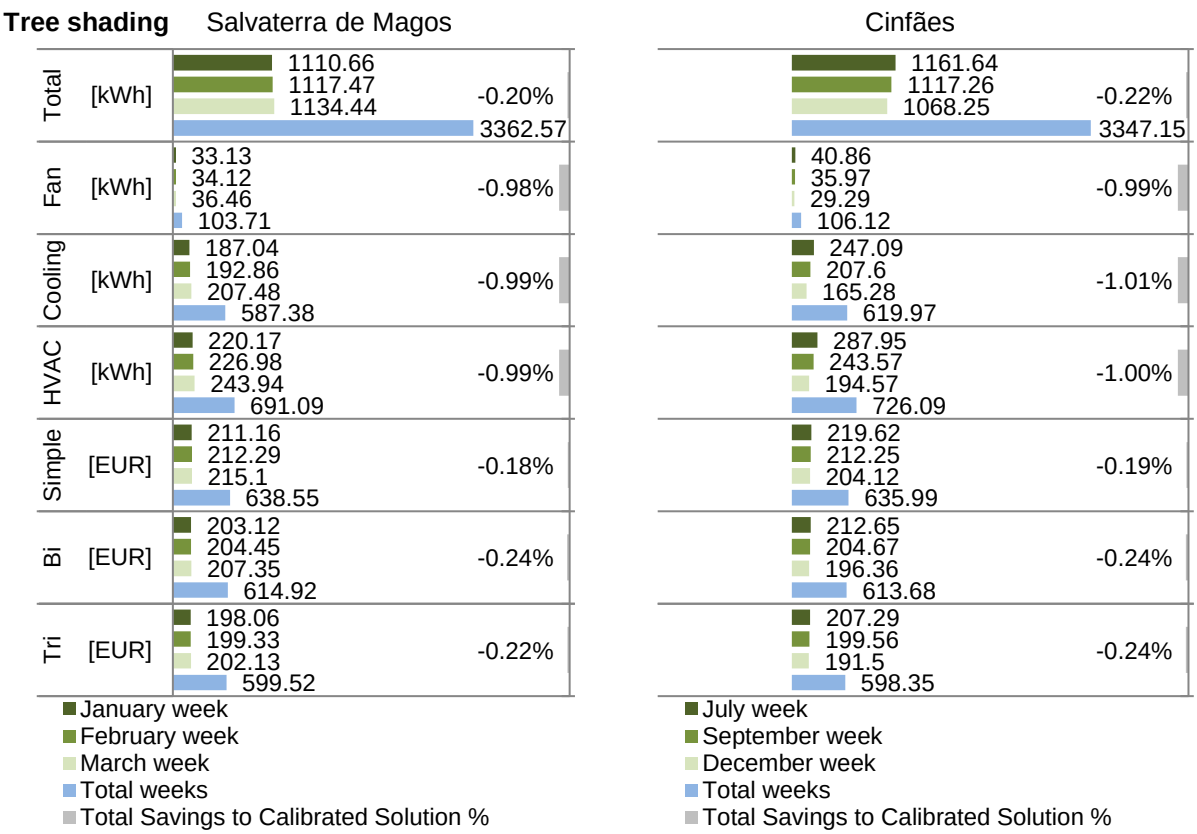

Figure 5-6: Optimization results for individual solution for Salvaterra de Magos (left) and Cinfaes (right): Shading by three pine trees. Overview of energy consumption (total facility/fan/cooling/HVAC) and energy costs (simple tariff/dual-rate tariff/tri-rate tariff) for week and total weeks time period. Each output includes actual savings [%] to calibrated solution for total weeks time period.

Considering the energy costs, the tri-rate tariff has the most favorable price: both locations have total energy costs of around 599 EUR, thus they save about 0.23% compared to the calibrated solutions.

5.3.4 Free Cooling with Economizer Function

The economizer function is a promising solution within the data center sector [71]. It allows to “free cool” the data center space with colder outside air. If the outside air is warmer and above the maximum set point, mechanical cooling is switched on. In EnergyPlus the HVAC module permits to add the economizer settings. The settings are summarized in Table 5-3. Dew point limitations may prevent high interior humidity (above 60% relative humidity). An upper limit of 20°C (dry bulb) should allow economizer to operate as long, as possible. Economizer lockout is not necessary, as there is no heat recovery system.

Table 5-3: Economizer settings of the HVAC in EnergyPlus

Parameter	Option
Type	Fixed Dew point and Dry bulb temperature
Lockout	No
Max. Dry bulb temperature	20°C
Max. Dew point temperature	13°C
Min. Dry bulb temperature	5°C

The simulation results for both containers are shown in Figure 5-7. Significant reductions in facility energy consumption of 7.05% are identifiable for Salvaterra de Magos, whereas Cinfães decreases its consumption by 3.50%, compared to its calibrated solution. As the economizer operates more time in Salvaterra de Magos, more fan energy is needed than in Cinfães. Thus, the fan energy is increasing by 71.88% in Salvaterra de Magos, whereas in Cinfães only by 31.18%, compared to the calibrated solution. At the same time, about half of the cooling energy is saved in Salvaterra de Magos: 52.72%. Therefore, the results demonstrate that the economizer function is most effective in winter periods.

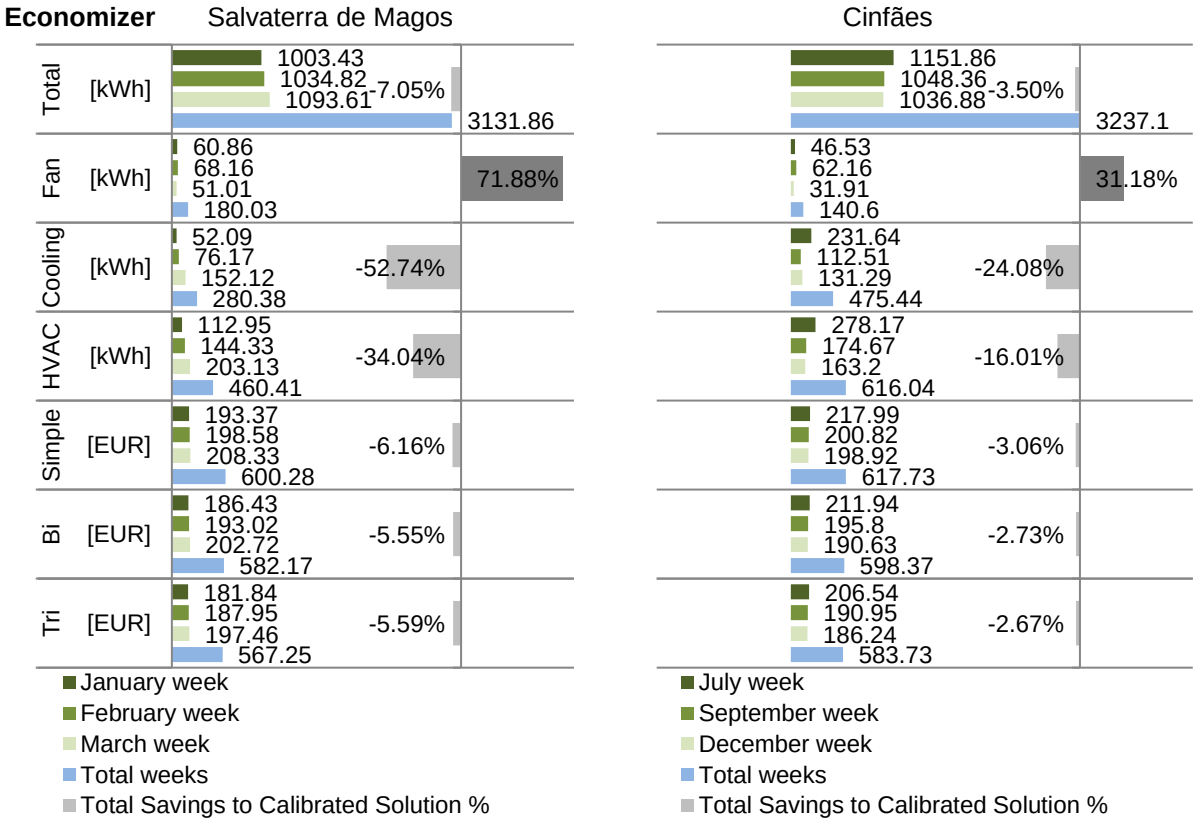

Figure 5-7: Optimization results for individual solution for Salvaterra de Magos (left) and Cinfaes (right): Economizer (with maximum outdoor air 20°C). Overview of energy consumption (total facility/fan/cooling/HVAC) and energy costs (simple tariff/dual-rate tariff/tri-rate tariff) for week and total weeks time period. Each output includes actual savings [%] to calibrated solution for total weeks time period.

Looking at the costs, substantial reductions may be achieved. As expected by the previous solutions, the tri-rate tariff is the most effective. Salvaterra de Magos has energy costs of 567 EUR, which is a reduction of 5.59% compared to the calibrated solution. Cinfães has costs of 583 EUR (savings of 2.67%) slightly more expensive than Salvaterra de Magos, due to the impact of the summer period.

5.3.5 Insulation Thickness

In this solution, the insulation thickness parameter is modified. The calibrated parameter for Salvaterra de Magos is 0.025 m and for Cinfães 0.030 m. The new thickness in this case is 0.001 m for both, which is practically a wall without insulation. Less insulation material is supposed to increase the transmission losses, except in time periods with hot outdoor temperatures (July/August). This is portrayed in the results in Figure 5-8, as the reductions in Salvaterra de Magos (mainly cold period) are 2.86%, which are slightly greater than in Cinfães (with 2.57%). At the same time, HVAC energy is reduced by 13.80% for Salvaterra de Magos and 11.74% for Cinfães, respectively. HVAC energy consumption for Cinfães is only higher in July, compared to the calibrated solution in July.

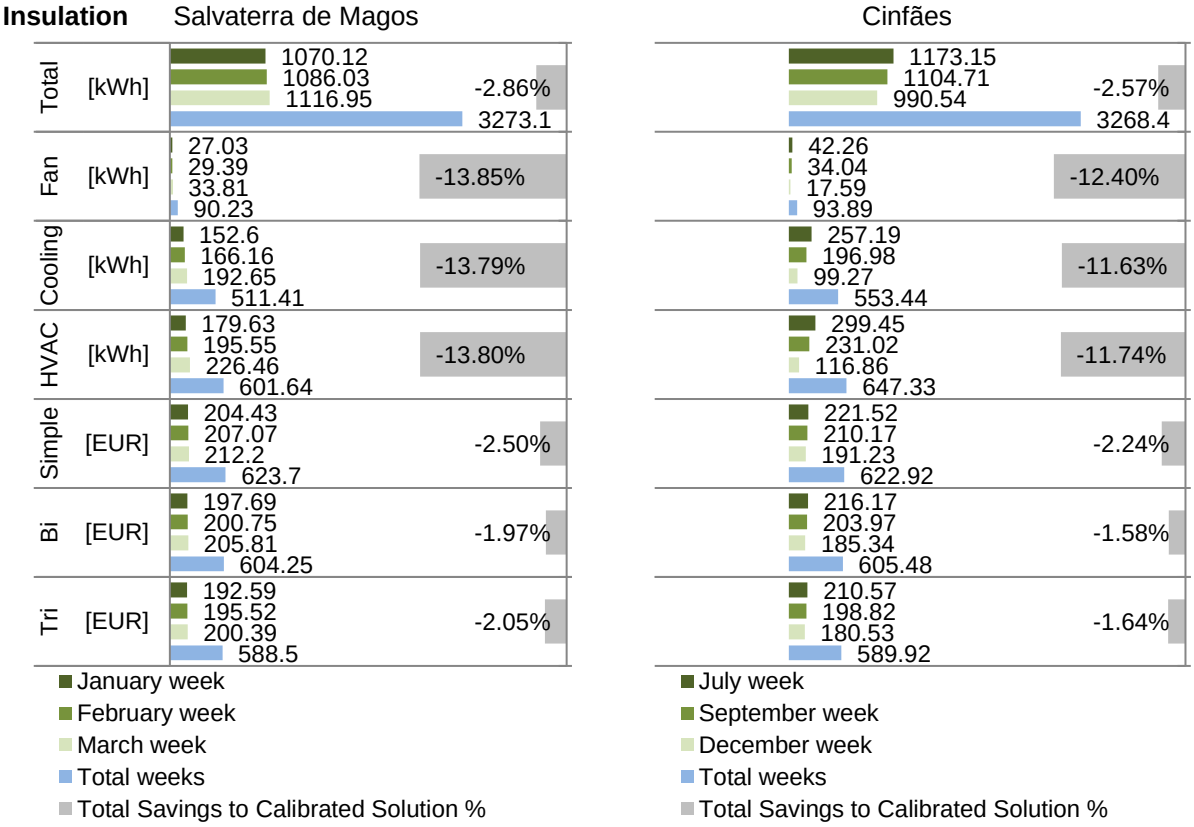

Figure 5-8: Optimization results for individual solution for Salvaterra de Magos (left) and Cinfaes (right): Insulation Replacement to 1 mm. Overview of energy consumption (total facility/fan/cooling/HVAC) and energy costs (simple tariff/dual-rate tariff/tri-rate tariff) for week and total weeks time period. Each output includes actual savings [%] to calibrated solution for total weeks time period.

The energy charges are again the lowest with the tri-rate tariff. For Salvaterra de Magos the price for three weeks period is 589 EUR (savings of 2.05%), while for Cinfães 590 EUR (savings of 1.64%).

Thus, reducing or removing the insulation may be a promising measure, especially in cases where internal heat gains are high and outdoor temperatures drops are moderate. Only in months with hot average outdoor temperatures (July) insulation reduction is not beneficial.

5.3.6 Temperature Set Point

As the ASHRAE standards (sub-chapter 2.2) allow a maximum interior temperature of 27°C, this solution proposes a conservative increase of the temperature set point to 25°C. This set point permits having container temperatures still in the sufficient range and may reduce cooling energy needs at the same time. Initial calibrated set points are 20.5°C for Salvaterra de Magos and 22°C for Cinfães. The results of the set point boost are shown in Figure 5-9. Due to the larger discrepancy of calibrated and new set point, Salvaterra de Magos reduces total consumption by 1.34%, which is higher than Cinfães with 0.98% of reductions. In other terms, HVAC energy is decreased by 6.47% and 4.46%, respectively.

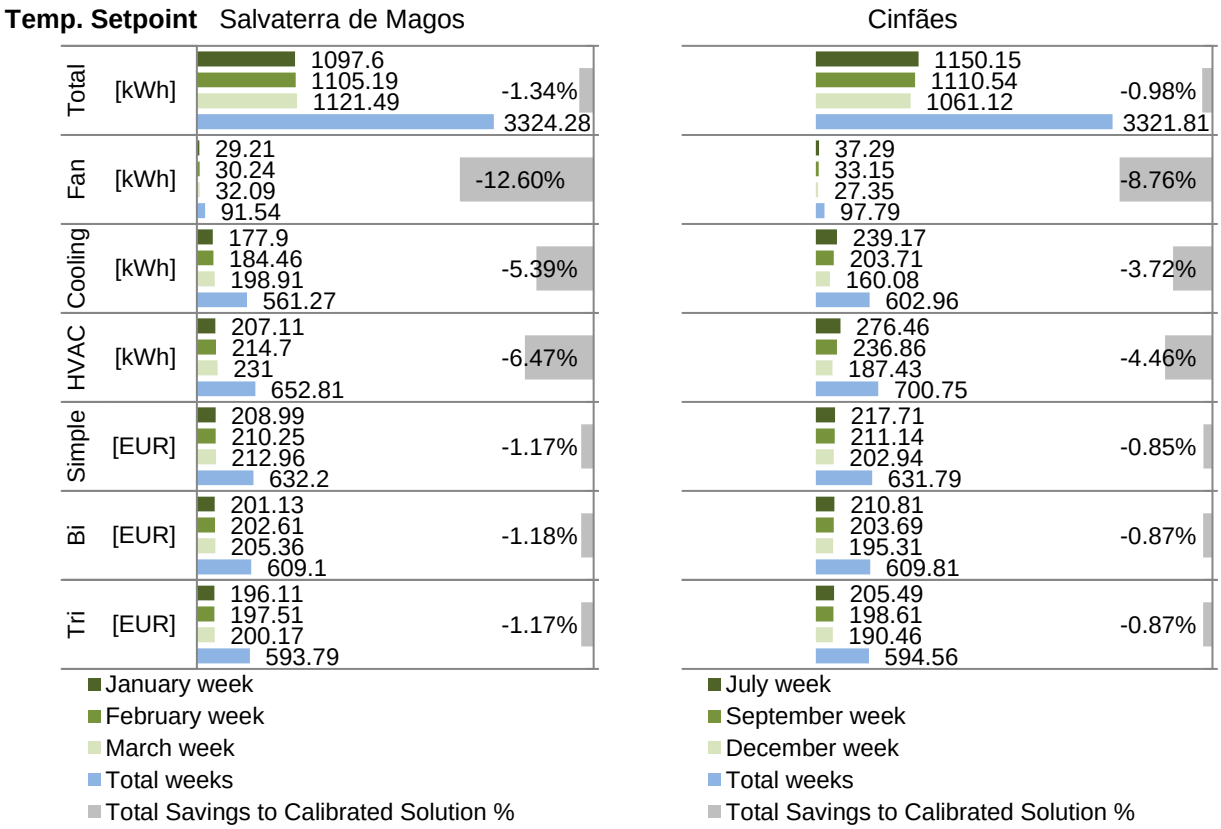

Figure 5-9: Optimization results for individual solution for Salvaterra de Magos (left) and Cinfaes (right): Temperature Setpoint at 25 °C. Overview of energy consumption (total facility/fan/cooling/HVAC) and energy costs (simple tariff/dual-rate tariff/tri-rate tariff) for week and total weeks time period. Each output includes actual savings [%] to calibrated solution for total weeks time period.

The energy costs may be reduced by 1.17% for Salvaterra de Magos and 0.87% for Cinfães in the tri-rate tariff. In other words, the price to pay is 594 EUR and 595 EUR, respectively, in a run period of

three weeks. This solution is adaptable without significant efforts, as there are no material changes involved.

5.3.7 Demand-Response with Pre-Cooling

The last individual solution concerns a demand-response approach with pre-cooling of the containers. The idea of this strategy is to take advantage of the time-sensitive tariffs. The energy price [EUR/kWh] is lower in offset periods between 22 PM to 8 AM. Thus, the temperature set point is decreased to 15°C between 7 to 8 AM to pre-cool. In a next step, between 8 to 9 AM, the set point is raised to 28°C to reduce cooling. The objective is not a reduction in the energy consumption, but cutting of the costs in the time-sensitive tariffs. A complete HVAC switch-off is not achievable, due to the rapid increment of the container temperature.

In terms of facility energy consumption, the results in Figure 5-9 show, as anticipated, an increase in total consumption of 0.02% for Salvaterra de Magos and 0.04% for Cinfães, being rather balanced, compared to the calibrated solutions. HVAC energy also rises slightly in both locations.

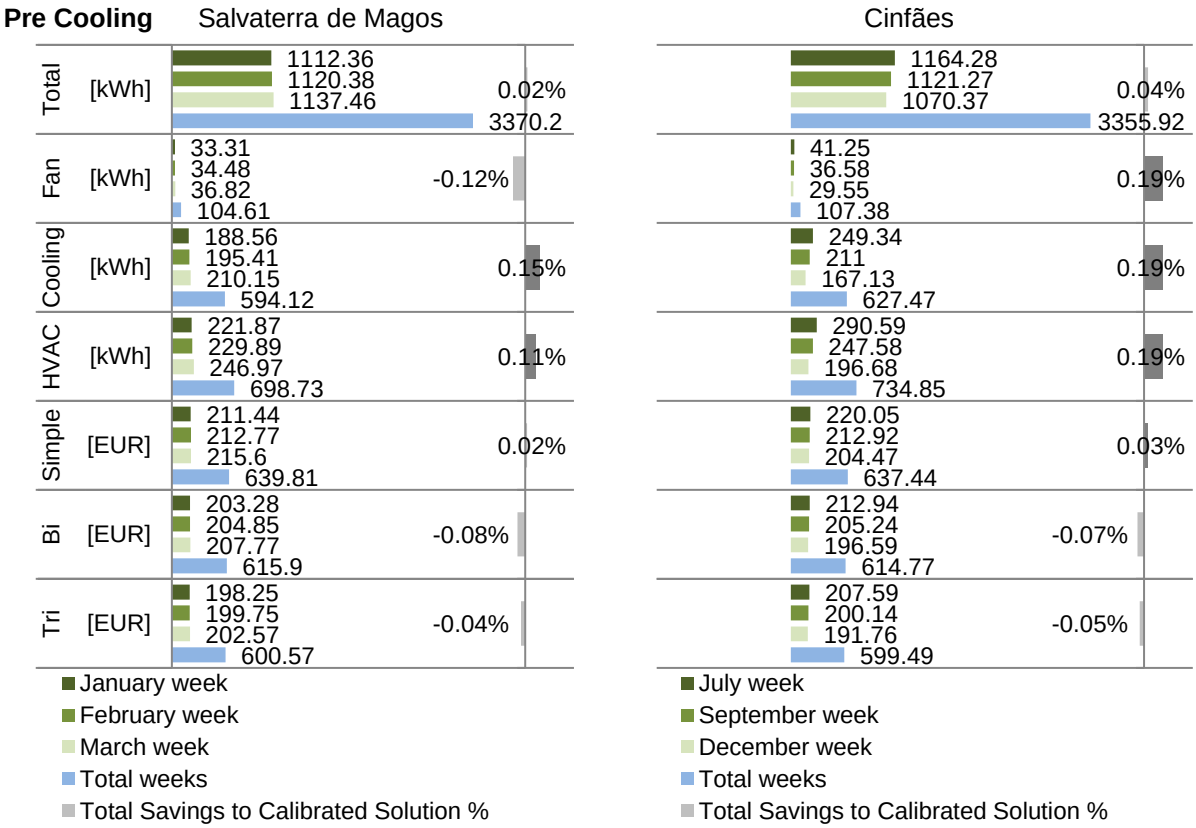

Figure 5-10: Optimization results for individual solution for Salvaterra de Magos (left) and Cinfaes (right): pre-cooling (7-8 AM: 15°C / 8-9 AM: 28°C). Overview of energy consumption (total facility/fan/cooling/HVAC) and energy costs (simple tariff/dual-rate tariff/tri-rate tariff) for week and total weeks time period. Each output includes actual savings [%] to calibrated solution for total weeks time period.

Regarding the costs, there is insignificant reduction in the tri-rate tariff in both cases. Salvaterra de Magos sees a reduction in costs by 0.04% and Cinfães by 0.05%. Consequently, the results for this demand response solution are inconvenient and the solution is not pursued in the optimization model.

5.3.8 Results Overview for Individual Solutions

This sub-chapter gives an overview of the obtained results in total energy savings and HVAC savings for the individual solutions. As plotted in Figure 5-11, the most promising solution in terms of HVAC savings is the economizer for both Salvaterra de Magos and Cinfães. In addition, it is a solution that is free of charge, as the function is already built in the containers. Looking at the total energy savings, the best solution for Cinfães is implementing photovoltaic panels. This may also be caused by the fact that Cinfães is partly simulated during summer time. Besides that, roof and tree shading has only a small effect on both total energy and HVAC savings.

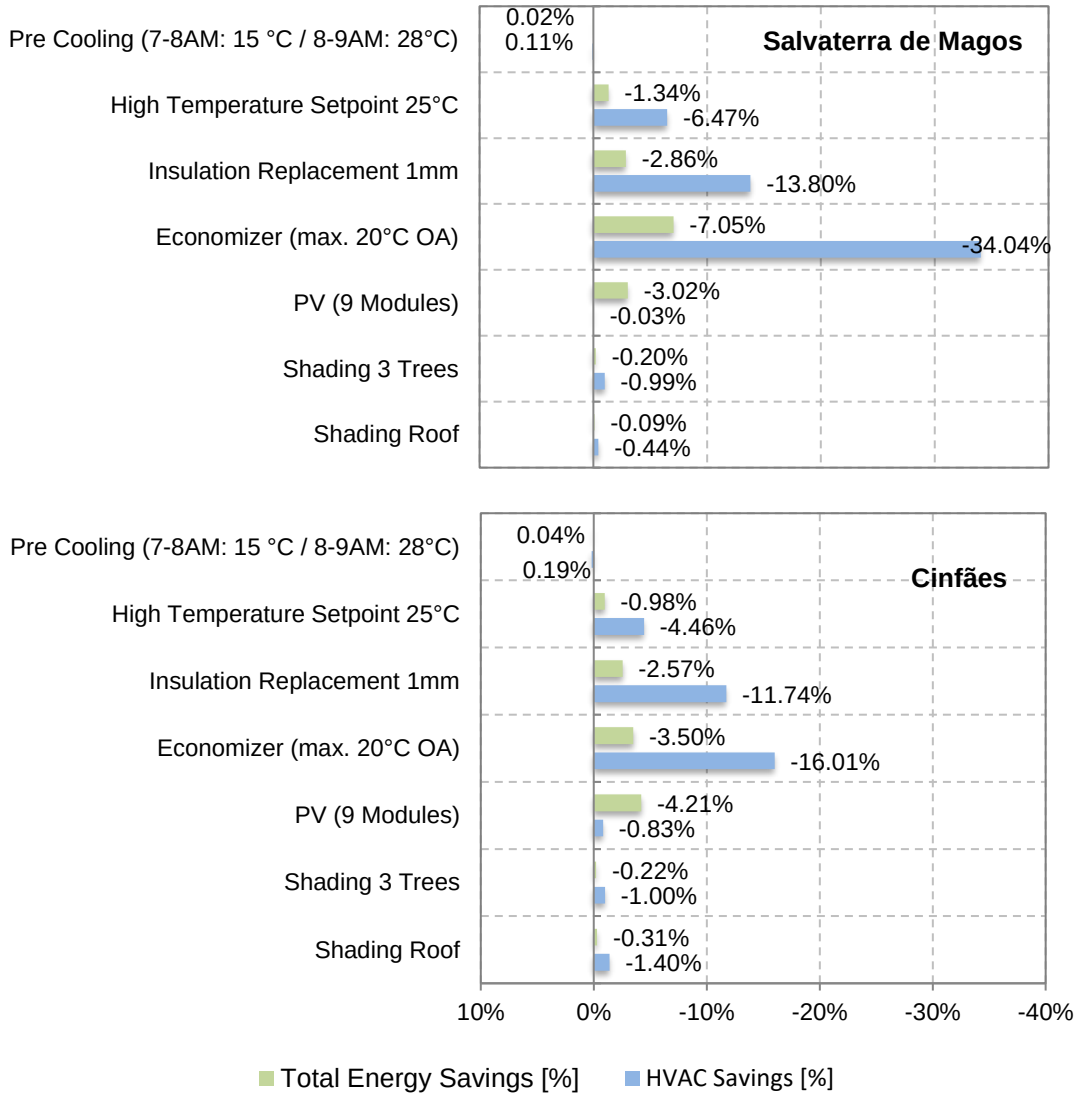

Figure 5-11: Results of individual solutions for Salvaterra de Magos and Cinfães: total facility energy savings [%] and HVAC energy savings [%] compared to calibrated solution for total three weeks time period.

Although being the solution with the highest saving potential, the reason why the economizer mode of the HVAC is not being used by the managers of these containers relates to the fact that the free-cooling systems' circuits were damaged. Therefore, the implementation of this solution in practice will require the balance between the costs of fixing that unknown problem and the calculated savings in this work.

5.4 Multi-Objective Optimization Models

In this sub-chapter, the design of the optimization models for Salvaterra de Magos and Cinfães is described and the results of the MOO runs are presented. The idea of the models is to join each individual solution into a combination of solutions to identify the Pareto optimal solutions with the best combinations. To display energy costs, the tri-rate tariff is implemented, as it is the most beneficial tariff as depicted in sub-chapter 5.3. The goal is to minimize both investment costs $C_{Investment}$ and energy costs C_{Energy}, which is described in the following multi-objective optimization problem (5.1):

$$\mathrm{Min}\{C_{Investment}(\vec{x}), C_{Energy}(\vec{x})\}, \vec{x} = [x_1, x_2 \dots x_m] \quad \textbf{(5.1)}$$

With:

$\vec{x}$ = Vector of the decision variables

m = Number of decision variables

Similarly to the individual solutions, the run period is three weeks. The models are created in a jEPlus project. The optimization is executed in jEPlus+EA, with simulation performed in EnergyPlus. The flowchart of the MOO run is shown in Figure 5-12, which is comparable to the process of calibration based on optimization. However, the objectives are different and are estimated by jEPlus+EA.

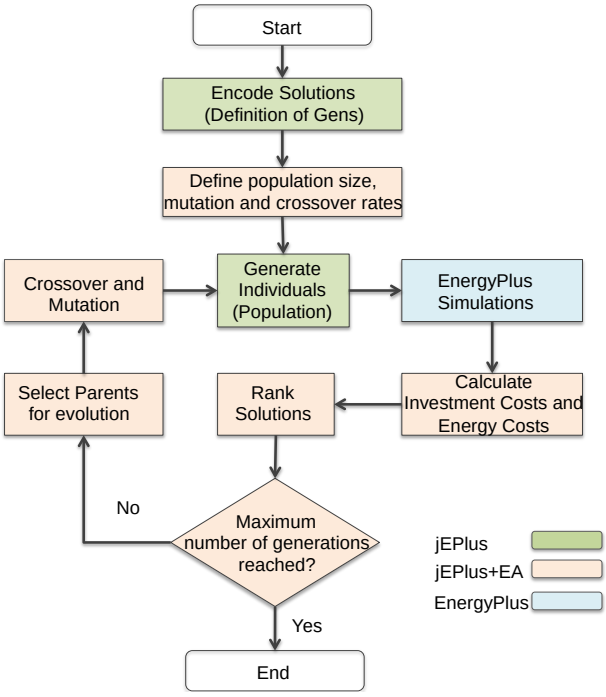

Figure 5-12: Flowchart of multi-objective optimization model

The six individual solutions are transformed in four parameters in jEPlus. The four parameters consist of three individual parameters and one combinatorial parameter (that combines 3 dependent parameters). The combinatorial parameter is created due to certain dependencies in the model. For instance, the combined solution of photovoltaic and tree shading is redundant, thus a combinatorial parameter prevents undesirable combinations. The parameter tree is pictured in Figure 5-13, including the combinatory structure of the parameters PV panel, roof shading and trees.

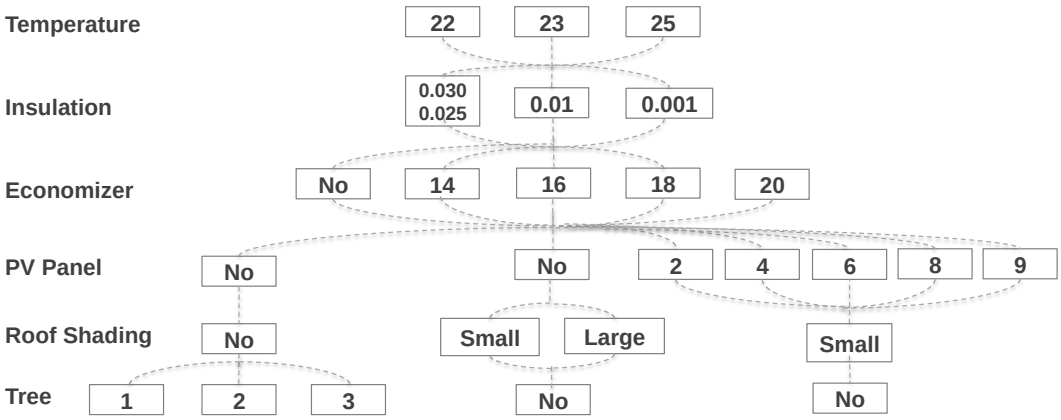

Figure 5-13: Parameter tree for multi-objective-models for both locations

The total solution space counts 495 possibilities. The maximum dry bulb temperature characterizes the economizer parameter. Numbers of PV panels vary between two and nine units. Roof shading device is extended by a “large” shading option, which is shown in Figure 5-14 and covers the total container land fenced area. The “small” solution remains the same. The quantity of trees ranges from one to three units.

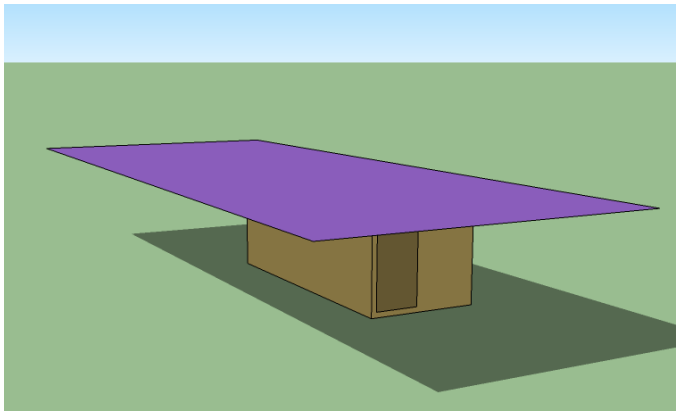

Figure 5-14: Roof shading device, large option

Investment costs for the models are estimated based on simplified assumptions and are presented in Table 5-4. Installation costs (for instance for PV Panels) are not considered, as they fluctuate much.

Table 5-4: Investment costs per unit of individual solution

Unit	Cost [EUR/unit]
1 PV Panel[3]	280
Roof shading (big)[4]	250
Roof shading (small)	50
1 Tree[5]	200
Insulation Change[6]	150

To create the MOO models, the function EP-Macro feature is used in jEPlus. The main advantage is the possibility of including external files, which contain pieces of model code, into the main EnergyPlus model code. This gives the possibility to define a block of code in the building model as one parameter in jEPlus. As an example, the numbers of trees are different geometric objects that cannot be changed by varying a single parameter. Thus, an individual program block is designed for each tree that is only included to the main program code if required.

5.5 Multi-Objective Optimization Results

The MOO models are created for both, Salvaterra de Magos and Cinfães. Thus, the optimization runs are performed twice. For demonstration purposes, the scatter plots for both are illustrated in Figure 5-15. The Pareto front is visible (red dots) with 11 solutions for Salvaterra de Magos and 8 solutions for Cinfães. The solutions with the lowest energy costs (but highest investment costs) are 520 EUR for Salvaterra de Magos and 530 EUR for Cinfães, corresponding to investment costs above 2500 EUR.

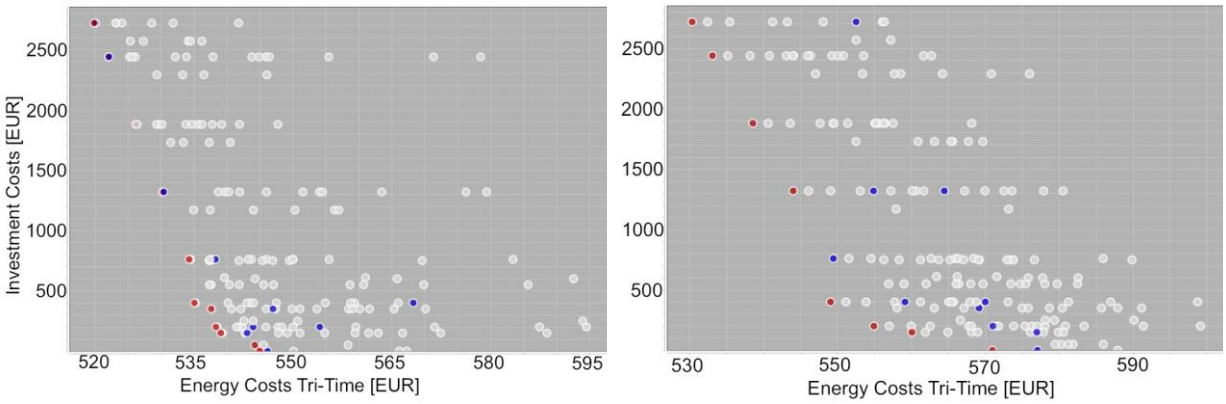

Figure 5-15: Scatter plot result in jEPlus+EA after 30 generations for Salvaterra de Magos (left) and Cinfaes (right): pareto front with two objectives, minimization of investment costs (y-axis) and energy costs in tri tariff (x-axis). Red dots are Pareto optimal solutions and blue dots are solutions of the last generation.

[3] An online shop offered this panel for a slightly cheaper price of 250 EUR [72]
[4] Corrugated iron with a price of approximately 3.50 EUR/m^2
[5] Assuming the price for a transplantation of an adult tree
[6] Assuming the price for insulation removal of approximately 2 EUR/m^2

Table 5-5 gives a summary of the parameter variation of each Pareto optimal solution for Salvaterra de Magos. Each solution has 25°C as the maximum temperature set point. Economizer set point is spread between 18°C and 20°C. Most of the solutions have no insulation (0.001 m). Only one solution is equipped with a tree. All possible photovoltaic options are represented in the results. Besides that, both, small and large, roof-shading devices are also part of the Pareto front.

Table 5-5: Overview of Pareto optimal solutions of Multi-Objective Optimization for Salvaterra de Magos

Pareto Optimal Solution	Insulation Thickness [m]	Economizer Set point [°C]	Temperature Set point [°C]	PV Panels	Roof Shading	Trees
G-0_2_4_2_0	0.025	20	25	0	No	0
G-0_2_4_2_4	0.025	20	25	0	Small	0
G-0_0_3_2_0	0.001	18	25	0	No	0
G-0_0_3_2_4	0.001	18	25	0	Small	0
G-0_0_4_2_1	0.001	20	25	0	No	1
G-0_0_3_2_5	0.001	18	25	0	Large	0
G-0_0_3_2_6	0.001	18	25	2	Small	0
G-0_0_3_2_7	0.001	18	25	4	Small	0
G-0_0_3_2_8	0.001	18	25	6	Small	0
G-0_0_4_2_9	0.001	20	25	8	Small	0
G-0_0_4_2_10	0.001	20	25	9	Small	0

In Table 5-6, the Pareto optimal solutions for Cinfães are presented. Each solution has an economizer set point of 18°C and container temperature set point of 25°C. Insulation is removed in all cases, with exception of a single solution. Small and large roof shading devices and all quantities of PV panels are part of the Pareto front. There is no solution with trees.

Table 5-6: Overview of Pareto optimal solutions for Multi-Objective Optimization for Cinfaes

Pareto Optimal Solution	Insulation Thickness [m]	Economizer Set point [°C]	Temperature Set point [°C]	PV Panels	Roof Shading	Trees
G-0_2_4_2_0	0.030	20	25	0	No	0
G-0_0_4_2_0	0.001	20	25	0	No	0
G-0_0_4_2_4	0.001	20	25	0	Small	0
G-0_0_4_2_5	0.001	20	25	0	Large	0
G-0_0_4_2_7	0.001	20	25	4	Small	0
G-0_0_4_2_8	0.001	20	25	6	Small	0
G-0_0_4_2_9	0.001	20	25	8	Small	0
G-0_0_4_2_10	0.001	20	25	9	Small	0

To obtain an idea about the cost relationships within the solutions, Figure 5-16 shows the investment costs, the savings to calibrated solutions (simple time tariff) and the energy savings to calibrated solutions for each Pareto optimal solution. The investment costs range from 0 to 2720 EUR for Salvaterra de Magos. The monetary difference in terms of savings between the “cheapest” and “most expensive” solution is only 25 EUR. However, savings are 95 EUR (14.81%) for the “cheapest” and 120 EUR (18.74%) savings for the “most expensive” solution. Energy consumption savings compared to the calibrated solutions vary between 10.8% to 15.2% in the best case.

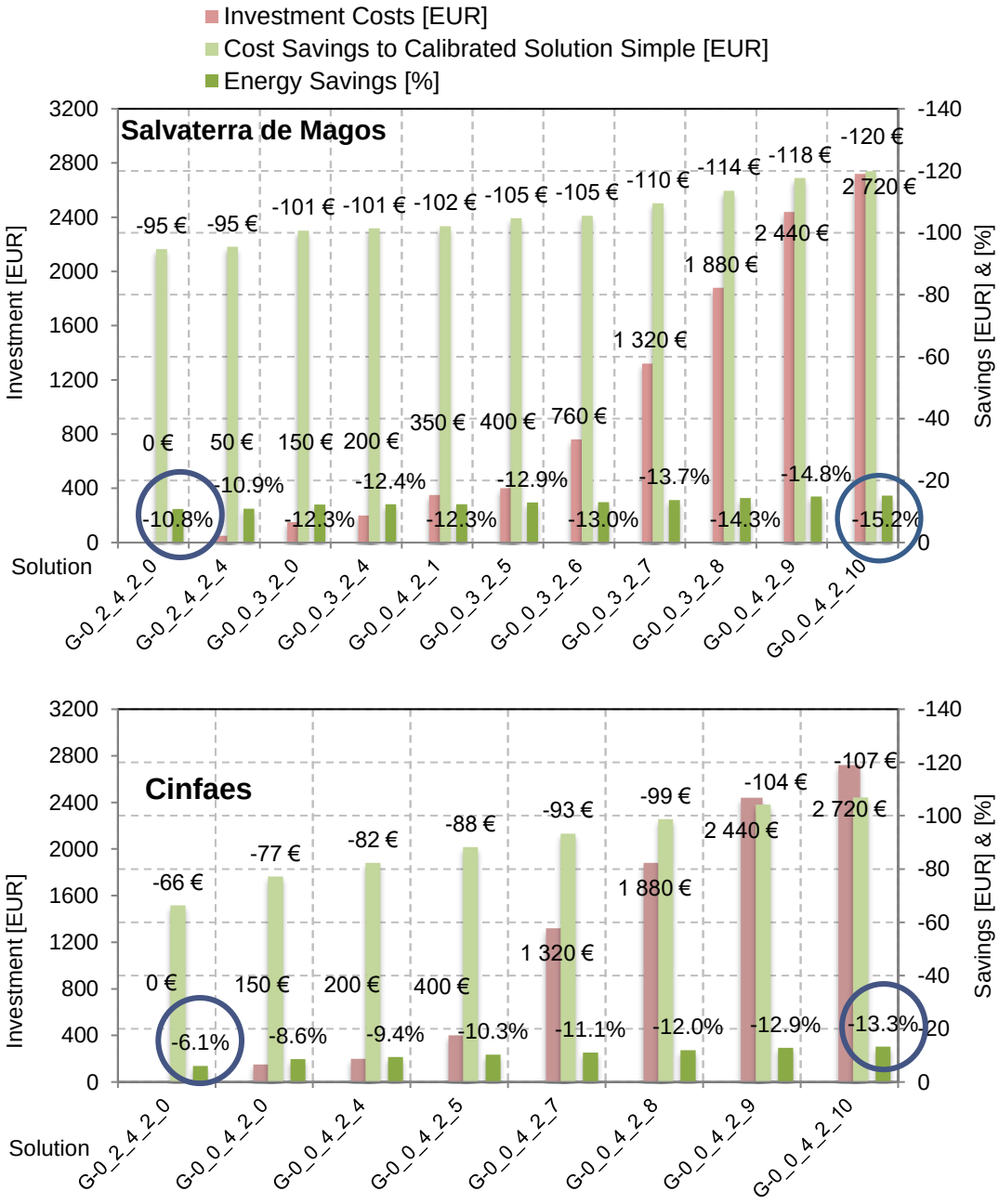

Figure 5-16: Results of the multi-objective optimization model (tri-rate tariff) for Salvaterra de Magos and Cinfães: comparison of investment costs and savings of the Pareto optimal solutions. Cost savings and energy savings compared to the calibrated solutions (simple tariff)

For Cinfães, results are quite similar, although total energy savings are smaller, compared to Salvaterra de Magos. Here, the “cheapest” solution can make up savings of 66 EUR (10.40%) compared to the calibrated solution in the simple tariff, whereas the “most expensive” solution reduces the total costs by 107 EUR (16.78%). Here, energy consumption savings differ from 6.1% to 13.3%.

In summary, the combination of economizer utilization, increment of temperature set point and insulation reduction may be promising optimization measures for both container locations. Optional PV panel, especially in summer months, can significantly reduce facility energy consumption. The shading alternatives may be beneficial, but are especially integrated in the optimization model to show a wider range of practical solutions.

It should be noticed, that the entire optimization is based on three weeks. Therefore, savings over a year period may be significant higher. As the calibrated solutions are the basis for savings comparisons, it is difficult to scale the results from a three weeks period up to a year period.

6 Conclusion and Future Work

The implementation of Modular Data Centers (MDCs) for ICT purposes has been an ongoing trend over the last decade, especially caused by the increasing demand for cloud-based storage. Those facilities require large cooling needs that need to be constantly satisfied by a HVAC system. Thus, they have an enormous potential for intelligent energy reduction measures.

The present work proposed to create and calibrate four thermal simulation models for different containerized MDCs in remote locations within Portugal. Information about ICT equipment and air conditioning settings were not available. After designing a model for each facility, two MDCs with identical geometries were successfully calibrated. Based on their calibrated parameter information, the facilities' energy performances were improved with the advantage of multi-objective optimization (MOO) models.

Two principal geometries of the MDCs were identified. Two locations (Cinfães, Salvaterra de Magos) have a larger size (20 ft.) size and the remaining ones (Montalegre, Mourão) have a smaller geometry (10 ft.), which depend on the ICT equipment power requirements for each location. Generally, direct expansion packaged systems are used to remove their heat loads. For accurate calibration purposes, suitable weather files from actual weather data were created. The thermal simulation models were designed with the software EnergyPlus. Except interior temperature measurements, total energy consumption measurements and HVAC datasheets, very little information on the actual cases was available. Thus, in cases without available data, for instance HVAC set points or material properties, the models' input is based on the author's subjective assumptions. Thus, the models are subject to relatively high uncertainties. Important assumptions in the models are the internal gains of the ICT equipment, which were supposed to be constant over time. The interior temperature set points were adjusted according to the measured values.

Once the models were designed, they were manually calibrated in a first approach. A modified operative temperature value was used for calibrating the interior temperature, as it was assumed that the temperature sensors measure some radiative part. The objective of the manual calibration was to identify graphically the fitting of measurement and simulation values of both, temperature and energy consumption. The measured and simulated values for the large container geometries were graphically balanced, so that the next step could be the automated calibration. However, large discrepancies were identified between measured and simulated energy consumption for the small container geometries. Thus, those two locations were not taken into further consideration in the automated model calibration.

The automated model calibration was performed with two different approaches to show their advantages and disadvantages. On the one hand, a parametric analysis was executed, which gives a complete picture of all the solutions, but which is very time consuming. On the other hand, an optimization with evolutionary algorithms approach is used, which obtains results much faster and

which requires less resources. Thus, the thermal simulation models were employed in the software package jEPlus (parametric analysis) and jEPlus+EA (optimization). Both approaches could identify the solutions that calibrate the models with the highest accuracy. To assess the performance of the calibration, two error indices were utilized: sum of CV(RMSE) and sum of NMBE. The calibrated time period of measurements and simulation was set in three weeks with hourly values. In each case, the sum of temperature and energy consumption error were taken. The calibration of Salvaterra de Magos resulted in a sum of CVRMSE of 10.23% and sum of NMBE of 1.43%, while Cinfães reached indices of 7.22% and 0.72%.

The sensitivity analysis focused on investigating the relative importance of the calibration design variables. When calibrating a model, it is very advantageous to know which of the parameters have the greatest impact and which ones are less influential on the calibration output. Both methods consider the temperature set point as the most influential input factor on the temperature calibration. Regarding the total energy consumption calibration, Morris and Sobol method agree that the ICT equipment power variable has the most impact. Infiltration rate has no influence at all in the calibration of both outputs. Two sensitivity methods were used, to compare the results accuracy. The Morris method offered what seems to be the best cost-benefit, as it requires less simulation time. It provided good qualitative data about the sensitivity of the input factors with low computational cost. The Sobol method showed great capability to estimate in a detailed and quantitative way the impact of the input factors. However, high computational costs are an important disadvantage of this method.

The calibrated solutions of the thermal models of Salvaterra de Magos and Cinfães were used to create MOO models. Initially seven individual solutions to improve the energy performance of the MDCs were determined: pre-cooling, higher temperature set point, insulation reduction, economizer function, photovoltaic modules, tree shading and roof shading. The three most promising solutions in both locations are economizer function (3.50% to 7.05% energy consumption reductions compared to calibrated solutions), photovoltaic modules (3.02% to 4.21%) and insulation reduction (2.57% to 2.86%). The application of pre-cooling in off-peak time tariffs was identified to be unbeneficial due to the constant high heat loads.

Subsequently, MOO models were created with the remaining six individual solutions as decision variables with two minimization objectives: investment costs and energy costs. To display energy costs, time-sensitive tariffs were implemented in the simulation models. Investment costs were estimated based on simple assumptions. The result of the optimization approach was in each case a Pareto front with various Pareto optimal solutions. Best results in terms of energy consumption savings compared to calibrated solutions are 15.18% for Salvaterra d Magos and 13.29% for Cinfães, which are energy cost reductions of 120 EUR (18.74%) and 107 EUR (16.78%), respectively. Both solutions consider investment costs of 2720 EUR. On the other end, the cheapest solution, which is free of charge in both cases, has energy consumption cutbacks of 10.82% for Salvaterra de Magos and 6.06% for Cinfães. This corresponds to energy costs savings of 95 EUR (14.81%) and 66 EUR

(10.40%), respectively. To conclude, MDCs offer great opportunities to decrease energy costs without making significant investments. Immediate adjustments of settings, for instance a tariff change from simple to tri-rate and utilization of free-cooling function, may lead to rapid savings in energy consumption.

Future work may involve another more detailed consideration of calibration and optimization. Expanding the time period of the optimization simulations from a three-week period up to a one-year-period could be beneficial. This should lead to a more complete insight in the economic paybacks. Having an idea about the payback periods of the individual solutions could be attractive. This involves furthermore a more comprehensive tabulation of the investment costs. Another look should be invested on the calibration of the small containers, as their calibration could not be successfully completed in this study. Moreover, the implementation of immediate measures in practice, such as free cooling or an increased temperature set point, may be motivating to verify the simulations, providing that the proper practical conditions in each container permit the implementation of those solutions.

References

[1] G. Cook and J. Van Horn, “How dirty is your data?,” *Greenpeace Int.*, 2011.

[2] M. G. Txapartegi and M. D. Eric, “New Technologies and Architectures for Efficient Data Centers,” 2015.

[3] M. Acton, P. Bertoldi, J. Booth, S. Flucker, L. Newcombe, and A. Rouyer, “2017 Best Practice Guidelines for the EU Code of Conduct on Data Centre Energy Efficiency,” 2017.

[4] European Comission, “An EU Strategy on Heating and Cooling,” Brussels, 2016.

[5] David Chernicoff, “Sun’s Datacenter container - forgotten, but not gone | ZDNet.” [Online]. Available: http://www.zdnet.com/article/suns-datacenter-container-forgotten-but-not-gone/. [Accessed: 15-Sep-2017].

[6] “Microsoft’s Next-Generation Data Centers | Data Center Knowledge.” [Online]. Available: http://www.datacenterknowledge.com/microsofts-next-generation-data-centers. [Accessed: 15-Sep-2017].

[7] Rich Miller, “Google Unveils Its Container Data Center | Data Center Knowledge,” 2009. [Online]. Available: http://www.datacenterknowledge.com/archives/2009/04/01/google-unveils-its-container-data-center. [Accessed: 15-Sep-2017].

[8] “Modular Data Centers — Huawei products.” [Online]. Available: http://e.huawei.com/en/products/network-energy/dc-facilities. [Accessed: 15-Sep-2017].

[9] “Scalable Modular Data Centres (MDCs) for Enterprise | HPE™ Portugal.” [Online]. Available: https://www.hpe.com/pt/en/integrated-systems/pods.html. [Accessed: 15-Sep-2017].

[10] Dell Inc, “Dell Modular Data Center,” 2011.

[11] “How to Enable Edge Computing Virtually Anywhere - Direct2DellEMC.” [Online]. Available: https://blog.dellemc.com/en-us/how-to-enable-edge-computing-virtually-anywhere/?newtab=true. [Accessed: 15-Sep-2017].

[12] M. Bramfitt and H. Coles, “Modular/Container Data Centers Procurement Guide: Optimizing for Energy Efficiency and Quick Deployment,” 2011.

[13] J. Hamilton, “An Architecture for Modular Data Centers,” in *3rd Biennial Conference on Innovative Data Systems Research (CIDR)*, 2007, pp. 306–313.

[14] W. Torell, “Types of Prefabricated Modular Data Centers,” 165, 2013.

[15] L. Ling, Q. Zhang, Y. Yu, and S. Liao, “Experimental investigation on the thermal performance of water cooled multi-split heat pipe system (MSHPS) for space cooling in modular data centers,” *Appl. Therm. Eng.*, vol. 107, pp. 591–601, 2016.

[16] H. Geng, *Data Center Handbook*. Wiley, 2015.

[17] ASHRAE Technical Committee 9.9, *Thermal Guidelines for Data Processing Environments*. 2011.

[18] “Applying 2011 ASHRAE data center guidelines to HP ProLiant-based facilities,” 2012.

[19] B. L. Marshall, “Transient CRAC Failure Analysis,” *Appl. MAth Model.*, pp. 1–7, 2010.

[20] P. Lin, S. Zhang, and J. VanGilder, “Data Center Temperature Rise During a Cooling System Outage,” *White Pap.*, vol. 179, pp. 1–13, 2014.

[21] Y. Joshi, P. Kumar, B. Sammakia, and M. Patterson, *Energy efficient thermal management of data centers*. 2012.

[22] T. Evans, “Fundamental Principles of Air Conditioners for Information Technology Executive Summary,” 2007.

[23] T. Evans, “The Different Technologies for Cooling Data Centers,” *Schneider Electr. White Pap. 59*, vol. 2, pp. 1–16, 2012.

[24] Siemon, “Maximizing power efficiency through smart planning and design Addressing Cabling and Pathways,” 2013.

[25] R. Khalid, “MS Thesis: Transient and Steady-State Thermodynamic Modeling of Modular Data Centers,” no. May, 2016.

[26] R. Brink, “Asperitas Immersed Computing,” Haarlem, 2017.

[27] W. Lintner, B. Tschudi, and O. VanGeet, “Best Practices Guide for Energy-Efficient Data Center Design,” *U.S Dep. Energy*, no. March, p. i-24, 2011.

[28] S. Greenberg, E. Mills, B. Tschudi, and L. Berkeley, “Best Practices for Data Centers : Lessons Learned from Benchmarking 22 Data Centers T,” *Aceee*, pp. 76–87, 2006.

[29] US Department of Energy, “EnergyPlus Engineering Reference: The Reference to EnergyPlus Calculations,” *US Dep. Energy*, pp. 1–847, 2010.

[30] Google, “Google Maps,” 2017. [Online]. Available: https://www.google.com/maps/. [Accessed: 23-Sep-2017].

[31] Panasonic, “Panasonic Develops Stand-Alone Power Supply Container for Areas Without Electricity | Panasonic Newsroom Global,” 2014. [Online]. Available: http://news.panasonic.com/global/topics/2014/26591.html. [Accessed: 23-Sep-2017].

[32] NREL National Renewable Energy Laboratory, “DView,” 2017. [Online]. Available: https://beopt.nrel.gov/downloadDView#hourly. [Accessed: 26-Nov-2017].

[33] U.S. Department of Energy, “EnergyPlus Downloads,” 2017. [Online]. Available: https://energyplus.net/downloads. [Accessed: 25-Sep-2017].

[34] OpenStudio, “OpenStudio Downloads,” 2017. [Online]. Available: https://www.openstudio.net/downloads. [Accessed: 25-Sep-2017].

[35] Big Ladder Software, “Elements Software,” 2017. [Online]. Available: http://bigladdersoftware.com/projects/elements/. [Accessed: 25-Sep-2017].

[36] LNEG - Laboratório Nacional de Energia e Geologia, “LNEG CLIMAS-SCE,” 2014. [Online]. Available: http://www.lneg.pt/servicos/328/2263/. [Accessed: 25-Sep-2017].

[37] National Environmental Satellite Data And Information Service (NOAA), “NNDC Climatic Data Online,” 2017. [Online]. Available: https://www7.ncdc.noaa.gov/CDO/cdopoemain.cmd?datasetabbv=DS3505&countryabbv=&georegionabbv=&resolution=40. [Accessed: 26-Sep-2017].

[38] meteoblue, “meteoblue Weather archive,” 2017. [Online]. Available: https://www.meteoblue.com/en/weather/forecast/archive/cinfães_portugal_2733963. [Accessed: 26-Sep-2017].

[39] Copernicus Atmosphere Monitoring Service, “CAMS radiation service,” 2017. [Online].

Available: http://www.soda-pro.com/web-services/radiation/cams-radiation-service. [Accessed: 26-Sep-2017].

[40] Lawrence Berkeley National Laboratory, “DOE2.1E-053 source code,” 1994.

[41] G. N. Walton, “Thermal Analysis Research Program (TARP) Reference Manual,” *Natl. Bur. Stand.*, pp. 43–50, 1993.

[42] R. Fragoso, “Energy Efficiency in Buildings in Portugal using the Energy Performance Certification System,” 2012.

[43] Rittal, “Data Center Container DCC,” 2017. [Online]. Available: https://www.rittal.com/de-de/product/show/variantdetail.action?productID=7857965. [Accessed: 01-Oct-2017].

[44] greenspec, “Insulation materials and their thermal properties,” 2017. [Online]. Available: http://www.greenspec.co.uk/building-design/insulation-materials-thermal-properties/. [Accessed: 01-Oct-2017].

[45] BASIX, “Solar absorptance - BASIX (Building Sustainability Index),” 2017. [Online]. Available: https://www.basix.nsw.gov.au/basixcms/thermal-help/design-principles2/insulation/roof-solar-absorptance.html. [Accessed: 01-Oct-2017].

[46] ISO, “ISO 13790:2008 Energy Performance of Buildings—Calculation of Energy Use for Space Heating and Cooling,” Geneva, 2008.

[47] The Concrete Centre, “Thermal Mass Explained,” *Wookware.Org*, p. 16, 2009.

[48] ASHRAE, “Nonresidential Cooling and Heating Load Calculation Procedures,” *ASHRAE Fundam. Handb.*, p. 29.1-29.40, ISBN:978-1883413880, 2001.

[49] L. Ng, “Infiltration in Energy Modeling : A Simple Equation Made Better,” *ASHRAE J.*, vol. 56, no. 7, pp. 70–72, 2016.

[50] J. O. Mundy and K. Livesey, “Environmental Design - CIBSE Guide A,” 2015.

[51] U. of I. Integrated Design Lab, “Calculation Spreadsheets - BSUG20,” 2017. [Online]. Available: https://sites.google.com/site/idlbsug/modeling-resources/calculation-spreadsheets. [Accessed: 28-Sep-2017].

[52] D. Coakley, P. Raftery, and M. Keane, “A review of methods to match building energy simulation models to measured data,” *Renew. Sustain. Energy Rev.*, vol. 37, pp. 123–141, 2014.

[53] E. Fabrizio and V. Monetti, “Methodologies and advancements in the calibration of building energy models,” *Energies*, vol. 8, no. 4, pp. 2548–2574, 2015.

[54] J. Lebrun and P. Lacôte, “Temperature Sensors in HVAC systems,” Liège, 2005.

[55] J. Niu and J. Burnett, *Integrating radiant/operative temperature controls into building energy simulations*, vol. 104. 1998.

[56] J. L. Niu, D. Ph, and J. Burnett, “Integrating radiant / operative temperature controls into building energy simulations,” *ASHRAE Trans.*, vol. 104, pp. 210–217, 1998.

[57] ANSI/ASHRAE, “ASHRAE Guideline 14-2002 Measurement of Energy and Demand Savings,” *Ashrae*, vol. 8400, p. 170, 2002.

[58] J. H. Holland, “Adaptation in Natural and Artificial Systems,” *Ann Arbor MI Univ. Michigan Press*, vol. Ann Arbor, p. 183, 1975.

[59] A. Konak, D. W. Coit, and A. E. Smith, “Multi-objective optimization using genetic algorithms: A tutorial,” *Reliab. Eng. Syst. Saf.*, vol. 91, no. 9, pp. 992–1007, 2006.

[60] Y. Zhang and I. Korolija, “jEPlus - An EnergyPlus simulation manager for parametrics,” 2017. [Online]. Available: http://www.jeplus.org/wiki/doku.php. [Accessed: 10-Oct-2017].

[61] A. Seshadri, “A Fast Elitist Multiobjective Genetic Algorithm: NSGA-II.”

[62] Y. Zhang and I. Korolija, “jEPlus Simulation Server (JESS),” 2017. [Online]. Available: http://www.jeplus.org/wiki/doku.php?id=docs:jess_service. [Accessed: 10-Oct-2017].

[63] S. Yang, W. Tian, E. Cubi, Q. Meng, Y. Liu, and L. Wei, “Comparison of Sensitivity Analysis Methods in Building Energy Assessment,” in *Procedia Engineering*, 2016, vol. 146, pp. 174–181.

[64] M. D. Morris, “Factorial sampling plans for preliminary computational experiments,” *Technometrics*, vol. 33, no. 2, pp. 161–174, 1991.

[65] A. Saltelli, *Sensitivity Analysis In Practice: A Guide to Assessing Scientific Models*. 2004.

[66] I. M. Sobol’, “Sensitivity Estimates for Nonlinear Mathematical Models,” *Mathematical Modeling and Computational experiment*, vol. 1. pp. 407–414, 1993.

[67] EDP Energias de Portugal, “Tarifas Baixa Tensão Normal até 20,7kVA,” 2017. [Online]. Available: http://www.edpsu.pt/pt/particulares/tarifasehorarios/BTN/Pages/TarifasBTNate20.7kVA.aspx. [Accessed: 11-Oct-2017].

[68] National Renewable Energy Laboratory (NREL), “Libraries and Databases | System Advisor Model (SAM),” 2017. [Online]. Available: https://sam.nrel.gov/libraries. [Accessed: 18-Oct-2017].

[69] SMA, “SMA Sunny Design Web,” 2017. [Online]. Available: https://www.sunnydesignweb.com/sdweb/. [Accessed: 18-Oct-2017].

[70] M. Chagolla and G. Alvarez, “Effect of Tree Shading on the Thermal Load of a House in a Warm Climate Zone in Mexico,” *Asme 2012 …*, vol. 7, no. 1997, pp. 761–768, 2012.

[71] S. W. Ham, J. S. Park, and J. W. Jeong, “Optimum supply air temperature ranges of various air-side economizers in a modular data center,” *Appl. Therm. Eng.*, vol. 77, pp. 163–179, 2015.

[72] photovoltaik4all.de, “Solarworld SW 175 poly RMA 175Wp,” 2017. [Online]. Available: https://www.photovoltaik4all.de/offgrid-module/solarworld-sw-175-poly-rma-175wp. [Accessed: 30-Oct-2017].